AD-A164 229 CRACKING RESISTANCE IN A 45-INCH (114-MM) PLATE OF 1/1
7075-T7351 ALUMINUM ALLOY(U) NAVAL RESEARCH LAB
WASHINGTON DC G R YODER ET AL 12 DEC 85 NRL-MR-5699
UNCLASSIFIED F/G 11/6 NL

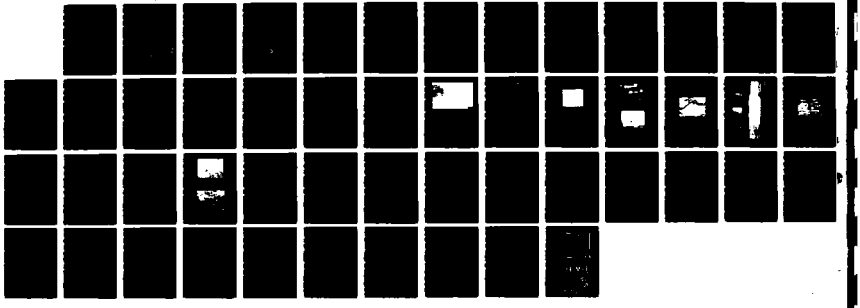

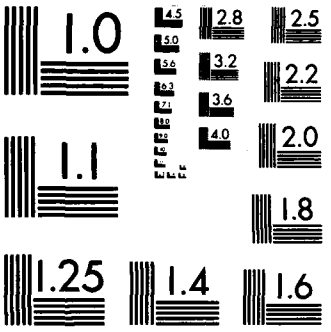

MICROCOPY RESOLUTION TEST CHART

(2)

NRL Memorandum Report 5699

Cracking Resistance in a 4.5-inch (114-mm) Plate of 7075-T7351 Aluminum Alloy

G. R. YODER, L. A. COOLEY, T. J. WATSON AND T. W. CROOKER

Mechanics of Materials Branch
Material Science and Technology Division

December 12, 1985

NAVAL RESEARCH LABORATORY
Washington, D.C.

SECURITY CLASSIFICATION OF THIS PAGE

AD-A164229

REPORT DOCUMENTATION PAGE

1a. REPORT SECURITY CLASSIFICATION UNCLASSIFIED	1b. RESTRICTIVE MARKINGS
2a. SECURITY CLASSIFICATION AUTHORITY	3. DISTRIBUTION/AVAILABILITY OF REPORT Approved for public release; distribution unlimited.
2b. DECLASSIFICATION/DOWNGRADING SCHEDULE	
4. PERFORMING ORGANIZATION REPORT NUMBER(S) NRL Memorandum Report 5699	5. MONITORING ORGANIZATION REPORT NUMBER(S)
6a. NAME OF PERFORMING ORGANIZATION Naval Research Laboratory 6b. OFFICE SYMBOL (If applicable) Code 6384	7a. NAME OF MONITORING ORGANIZATION
6c. ADDRESS (City, State, and ZIP Code) Washington, DC 20375-5000	7b. ADDRESS (City, State, and ZIP Code)
8a. NAME OF FUNDING/SPONSORING ORGANIZATION 8b. OFFICE SYMBOL (If applicable)	9. PROCUREMENT INSTRUMENT IDENTIFICATION NUMBER
8c. ADDRESS (City, State, and ZIP Code)	10. SOURCE OF FUNDING NUMBERS PROGRAM ELEMENT NO. / PROJECT NO. / TASK NO. / WORK UNIT ACCESSION NO. EX280-260

11. TITLE (Include Security Classification)

Cracking Resistance in a 4.5-inch (114-mm) Plate of 7075-T7351 Aluminum Alloy

12. PERSONAL AUTHOR(S)

Yoder, G.R., Cooley, L.A., Watson, T.J.,* and Crooker, T.W.

13a. TYPE OF REPORT	13b. TIME COVERED	14. DATE OF REPORT (Year, Month, Day)	15. PAGE COUNT
Final	FROM _____ TO _____	1985 December 12	50

16. SUPPLEMENTARY NOTATION *T.J. Watson, currently with the Reynolds Aluminum Co., Richmond, VA 23261, was affiliated with the Naval Research Laboratory at the time of this work.

17. COSATI CODES			18. SUBJECT TERMS (Continue on reverse if necessary and identify by block number)
FIELD	GROUP	SUB-GROUP	Aluminum alloys; Fracture toughness; Crack-like defects; Fatigue crack growth; Fatigue life; Shrinkage cavities

19. ABSTRACT (Continue on reverse if necessary and identify by block number)

After an anodizing treatment, peculiarities were observed in the appearance of structural components for the Space Shuttle, thought to be indicative of flaws in the Al-7075-T7351 material. Consequently, work was undertaken to explore structural integrity aspects of this material as well as the nature of any material defects. The material contains a number of macro- and microstructural inhomogeneities which could be classed as defects or potential crack-like defects, viz. stringers of brittle constituent particles, shrinkage cavities, and in one instance, a long line of sponge-like porosity. Nonetheless, uniaxial strength level was found to exceed design requirements. Similarly, results for cracking resistance — in terms of fracture toughness (K_{Ic}), fatigue crack growth rates (DA/DN) and rotating-beam fatigue life (S/N), appear to meet or exceed handbook levels. However, the very largest defects are so infrequently observed that their presence in the crack-tip process zone of an individual fracture mechanics specimen is something less than likely. The unusual macroappearance of anodized components may be attributable to entrapment of anodizing solution by microshrinkage cavities and/or microcracks along constituent particle stringer interfaces, with subsequent seepage and staining adjacent to these and/or other flaws.

20. DISTRIBUTION/AVAILABILITY OF ABSTRACT ☒ UNCLASSIFIED/UNLIMITED ☐ SAME AS RPT. ☐ DTIC USERS	21. ABSTRACT SECURITY CLASSIFICATION UNCLASSIFIED
22a. NAME OF RESPONSIBLE INDIVIDUAL G. R. Yoder	22b. TELEPHONE (Include Area Code) (202) 767-3571 22c. OFFICE SYMBOL Code 6384

DD FORM 1473, 84 MAR 83 APR edition may be used until exhausted. All other editions are obsolete.

SECURITY CLASSIFICATION OF THIS PAGE

CONTENTS

CRACKING RESISTANCE IN A 4.5-INCH (114-mm) PLATE OF 7075-T7351 ALUMINUM ALLOY

I. INTRODUCTION

During fabrication of hardware for the Space Shuttle program, a peculiarity was observed in the appearance of final-machined components of 7075-T7351 aluminum alloy following an anodizing treatment. Subsequent dye-penetrant inspection revealed surface markings which were particularly concentrated at the midthickness position of the 4.5-inch (114-mm) plate material. These markings were thought to be most likely indicative of a porosity problem. Consequently, an intensive study was immediately commenced to explore the structural integrity implications for this material as well as to further examine the nature of anticipated microstructural defects. The purpose of this report is to document the results from this study, including those concerning tensile strength, fracture toughness (K_{Ic}), fatigue crack growth rates (DA/DN) and fatigue life, as well as to characterize material defects.

II. MATERIAL AND PROCEDURE

A. Material Characterization

1. Chemical analysis

Several 4.5-inch plates of aluminum alloy 7075-T7351 were procured from Kaiser Aluminum in accord with Federal Specification QQ-A-250/12F. Chemical analyses of these plates were very similar; a typical example is as follows: 5.63Zn-2.40Mg-1.52 Cu-0.216Cr-0.087Fe-0.057Si-0.025Mn-0.015Ti-0.006Zr-Al (bal.). Unless otherwise specified, all further study was confined to a single plate.

Manuscript approved September 30, 1985.

2. Dye Penetrant Appearance

A color photograph of a saw-cut, through-thickness section of the plate is shown in Fig. 1, as observed with ultraviolet light. Note that apparent indications of defects are concentrated near the midthickness position.

3. Microstructure

a. As-polished condition

To examine the nature of the suspected porosity, as well as the constituent particle (inclusion) population, small metallographic samples were cut (~ 0.5-inch cube), mounted in bakelite and polished from 600 grit silicon carbide paper (17 μm) through 1200 grit paper (12-15 μm) followed by #3 diamond (3 μm) and #1/2 diamond (0.5 μm) slurries on a Buehler Texmet cloth.

(1) Constituent particles

Photomicrographs are compared in Figs. 2 and 3 for samples cut from the plate surface vs. midthickness locations, respectively, in the T-orientation (i.e. with the long transverse direction normal to the micrographs). The constituent particles and their associated stringers appear to be somewhat larger at the midthickness location. The length of individual particles has been observed to be as large as 45 μm, with associated stringers approaching 330 μm. A example of such a long stringer is shown in Fig. 3(b).

The primary type of constituent particle was examined in an electron probe x-ray microanalyzer. Results indicate substantial concentrations of Fe and Cu, cf. Fig. 4; and thus by reference to handbooks [1, 2], tentative identification is made of the intermetallic Al_7Cu_2Fe.

Of particular interest, it was observed that this species of constituent particle tends to crack very readily during metallographic

polishing. In fact, it was found that after conventional vibratory (automated) polishing with the 1.0 μm alumina paste, these particles exhibited substantial cracks - and in many instances, had shaken loose (at least in part) from the mounted sample, leaving voids as illustrated in Fig. 5. Only by hand-polishing with extraordinary care was it possible to avoid such behavior, cf. Fig. 6. The impact of such brittle cracking of these particles is of concern as regards the potential influence on mechanical properties/cracking resistance of the material.

(2) Shrinkage cavities

On infrequent occasions, defects much larger than the scale of constituent particle dimensions were observed. From their morphology, these appear to be rather gross shrinkage cavities - with dimensions as large as 0.016 inch (400 μm). It is difficult at this point to fully characterize the distribution of these very large cavities in the plate, as they have been observed in only three instances (all from the plate midthickness location) from among some two dozen or so metallographic samples. One of these shrinkage cavities is illustrated in Fig. 7. However, numerous other cavities similar in morphology but significantly smaller in dimension have also been observed.

On a machined surface, these shrinkage cavities can be made readily apparent by etching with a caustic reagent (NaOH aqueous solution) similar to that likely employed in operations (cleaning, etching, etc.) preparatory to the anodizing treatment itself. This point was confirmed in the laboratory through examination of a through - thickness section of the plate that had been belt ground to a relatively smooth finish (180 grit) and etched with NaOH aqueous solution.

Such microshrinkage cavities - as well as any microcracks along constituent particle interfaces, as described above - would seem to be potential sites for entrapment of the anodizing solution. One of the common anodizing solutions, chromic acid in particular, when entrapped by surface flaws during anodizing, is known to seep out and cause staining adjacent to the flaws [3], after removal of a piece from the anodizing bath and following washing and drying cycles. Perhaps this, or a similar sequence of events, could explain the macroappearance of the actual Shuttle components following the anodizing treatment. Visual examination of the actual Space Shuttle components in question by a knowledgable authority [4] has confirmed, with virtual certainty, the use of chromic acid in the anodizing solution.

(3) Other porosity

On one occasion, an even more gross defect was observed during the polishing of a 4-inch (102mm) x 6-inch (152mm) x 0.5-inch (12.7mm) sample with a 17 μm metallographic paper. In this instance, a long narrow band of porosity, spongelike in appearance, was observed. Its length measures nearly 0.7-inch (~ 18mm) in the S-orientation (i.e. thickness direction) - as illustrated in Fig. 8.

b. Polished and etched condition

The microstructure, as etched with Keller's reagent, is shown in Fig. 9 for the T-orientation at the plate midthickness location.

4. Hardness

The Rockwell B hardness was measured on a through-thickness section of plate (L orientation) to be 82.8 HRB near the surface of the plate, and a lesser level, 77.4 HRB at the midthickness location.

B. Determination of Mechanical Properties

1. Uniaxial tensile properties

Tensile properties for the L and T orientations were determined in accord with ASTM-E8 [5] using standard 0.505-inch (12.8mm) diameter specimens with a 2-inch (50.8mm) gage length. For the S-orientation, a subsized specimen was required; a diameter of 0.250-inch (6.35mm) and gage length of 1-inch (25.4mm) were employed.

2. Fracture toughness (K_{Ic})

Measurements of plane strain fracture toughness were made in accord with ASTM-E399 [6] for the LT, TL and ST orientations. For both the LT and TL orientations, determinations were made for locations adjacent to the plate surface as well as at midthickness. Specimens employed were of the standard compact tension type, with a one-inch (25.4mm) thickness. A loading rate corresponding to $\dot{K}$ = 50 ksi$\sqrt{in}$/min (55 MPa$\sqrt{m}$/min) was used.

3. Fatigue crack growth rates (DA/DN)

Fatigue crack growth rates in ambient air (~ 50 percent relative humidity) were determined in accord with ASTM-E647 [7] over a broad spectrum of stress intensity range (ΔK) levels. One-inch (25.4mm) thick compact tension specimens were examined for both the LT (plate midthickness location) and ST orientations. Specimens were cycled under constant load amplitude conditions using a haversine waveform, a stress ratio (i.e., ratio of minimum to maximum stress in fatigue cycle) of R = 0.08 and a frequency of 40 Hz. (At the upper end of the ΔK spectrum, the frequency was reduced to enhance load control.) Precision measurements of crack length (a) as a function of number of cycles were made using a compliance related clip-gage technique [8]. Data were reduced using the 7-point incremental polynomial method [7]. Supplementary data for the extreme low end of the ΔK spectrum were obtained from traveling microscope measurements at the specimen surface.

4. Fatigue life (S-N)

Determinations of fatigue life were made from rotating beam specimens (R = -1) with a one-inch (25.4 mm) gage length and a minimum diameter of 0.250-inch (50.8mm). These specimens, machined from plate surface and midthickness locations for both the L and T orientations, were polished longitudinally to a 400-grit surface finish. Specimens were cycled to failure at a frequency of approximately 200 Hz.

III. RESULTS

A. Uniaxial Tensile Properties

Uniaxial tensile properties are compared in Table 1 for the L and T orientations, as determined from standard sized (0.505-inch diameter) specimens. Results for the S-orientation are given in Table 2, as determined from subsized (0.250-inch diameter) specimens; these results include data obtained from a second plate of similar 4.5-inch material (designated plate "B"). Additionally, Table 2 shows limited data for the T (surface) orientation - which indicate that strength levels determined from the subsized specimens agree well with those obtained from the full sized specimens in Table 1.

Of prime importance, these data indicate that strength levels for all three orientations - whether from plate surface or midthickness ("center") locations, exceed both the design requirements for Shuttle application as well as material procurement specifications. Observed yield strengths range from 50.0 ksi (345 MPa) in the S-orientation to 59.3 ksi (409 MPa) in the L (center) orientation. Corresponding ultimate tensile strengths range from 60.7 ksi (419 MPa) (S-orientation, B plate) to 71.0 ksi (490 MPA) for the L (center) location. Tensile ductilities also exhibit significant orientation dependence, ranging from 9 percent R.A. (reduction-in-area) for the S-orientation (B plate) to 43% R.A. for L (surface); moreover, a surface to

center gradient is apparent - e.g. note the decrease to 30 percent R.A. for the L (center) location.

B. Fracture Toughness

Traces of load vs. crack-mouth-opening displacement for individual fracture toughness specimens are exhibited in Appendix A. Fracture toughness data determined from these individual plots are summarized in Table 3. These toughness data are clearly higher than reference to the Damage Tolerant Design Handbook [9] would suggest for this material. In fact, all of the data for the LT orientation - whether surface or center location, are so high as to exceed validity criteria* on the basis of specimen thickness. Yet handbook data suggests that a one-inch thickness would rarely fail to meet the validity criteria for plane strain crack tip constraint in this material.

For the primary plate examined (plate "A"), fracture toughness levels range from 31.9 ksi $\sqrt{in}$ (35.1 MPa$\sqrt{m}$) (invalid) for the ST orientation to 43.7 ksi $\sqrt{in}$ (48.0 MPa$\sqrt{m}$) (invalid) for the LT orientation. Valid K_{Ic} determinations were obtained for the TL orientation ("A" plate) and the ST orientation ("B" plate). Only small gradients in toughness are apparent from surface to midthickness locations in the A plate.

C. Fatigue Crack Growth Rates

Fatigue crack growth rates for the LT orientation, plate midthickness location (specimen no. ALT-3C) are shown in Fig. 10, where comparison is made to DA/DN levels from the Damage Tolerant Design Handbook [9]. Clearly, resistance to fatigue crack growth in the Shuttle material is at least as good or better than that suggested in ref. [9]. However, any apparent superiority may well be attributable to a frequency effect, since data

*Determinations of fracture toughness which fail to meet the validity criteria of ASTM-E399 may not bear any relation to a valid K_{Ic} measurement [6].

obtained at 40 Hz are compared to reference data for 6 Hz and 1 Hz.

Data for the ST orientation appear in Fig. 11, and are compared in Fig. 12 to those for the LT orientation. Clearly DA/DN levels for the two orientations are roughly the same over much of the ΔK spectrum, although the lower toughness associated with the ST orientation gives rise to an earlier onset to region III growth rate behavior [10, 11] and hence higher growth rates at the upper end of the ΔK spectrum. Tabulations of individual DA/DN data as a function of ΔK are given in Appendix B.

D. Fatigue Life

Rotating beam fatigue life ($R = -1.0$), as a function of orientation and plate surface vs. midthickness position, is summarized in Tables 4 and 5 for respective maximum stress levels of 40 ksi (276 MPa) and 50 ksi (345 MPa). At the 40 ksi level, fatigue life in plate A (average of 3 specimens) ranges from 155,033 cycles-to-failure in the S-orientation to 1,120,667 cycles in the T (surface) orientation. Owing to significantly greater ultimate tensile strength in the case of the latter, 69.6 ksi (480 MPa) vs. 61.4 ksi (423 MPa), the greater fatigue life would be anticipated. At the 50 ksi (345 MPa) maximum stress level, these same two orientations define the extrema in the data, but with lower fatigue lives of 50,233 cycles and 248,600 cycles, respectively. Notable reductions in fatigue life, in the range of 2- to 4-fold, are observed in going from surface to plate midthickness (center) locations for both the L and T orientations; the greatest reduction is by a factor of 3.7 for the T orientation at the 40 ksi (276 MPa) maximum stress level. Limited tests (S-orientation) with the second plate of material ("B") indicate very similar fatigue life to that measured for plate A.

The fatigue life data all compare favorably with those given in the Aerospace Structural Metals Handbook for this material [12], and in many

instances exceed the upper bound reference data. Of prime importance, even the minimum in fatigue life observed for the present material (viz. that for the S-orientation) substantially exceeds the cyclic life requirements for the Shuttle applications.

IV. DISCUSSION

Determinations of cracking resistance in this 7075-T7351 material, in terms of fracture toughness, fatigue crack propagation rate and rotating-beam fatigue life, all compare favorably with established handbook levels. Similarly, the measured uniaxial strength levels, regardless of plate surface or midthickness position, appear to exceed minimum requirements for the intended Shuttle application.

Nonetheless, some degree of caution is urged in interpretation of these results - inasmuch as it cannot be guaranteed that they reflect the worst-case behavior. To be specific, it is a matter of some concern that the very largest defects (such as the sizeable shrinkage cavities and the long narrow band of spongelike porosity) are so infrequently observed in this 4.5-inch plate that the statistical chance for one of them to be present, e.g. in the crack-tip process zone of an individual compact tension specimen, would appear to be very small.

On the other hand, it is felt that the somewhat surprisingly high levels of observed fracture toughness may actually reflect an enhancement attributable to some of the smaller-scale defects, such as the stringers of brittle constituent particles. These defects could well be expected to facilitate delamination in the rolling plane (S) for fracture toughness specimens of LT and TL orientation. Such delamination would then tend to subdivide the crack tip process zone into narrow strips through the thickness, giving rise to relaxed crack tip constraint on a localized basis - and thus, an apparently

enhanced toughness level. Preliminary examination of one of the compact tension specimen fracture surfaces in the scanning electron microscope appears to support this contention, as a number of secondary cracks along the S plane are apparent in the fracture zone of the LT toughness specimen exhibited in Fig. 13.

There is also another potential contributor to the high toughness levels, viz. the significant number of secondary, apparently crystallographic cracks in the region of the fatigue precrack. Inasmuch as degradation of fracture toughness from handbook levels was originally considered to be a possibility, compact tension specimens were fatigue precracked at ΔK levels well below upper-bound limits prescribed in ASTM-E647. Secondary, crystallographic cracks, which are characteristically observed at the lower end of the ΔK spectrum [13-15] might well lead to apparently higher toughness levels, owing to the bifurcated nature of the crack tip process zone. Preliminary evidence for such crystallographic bifurcation in the fatigue precrack region is exhibited in the scanning electron micrograph of Fig. 14 for an LT fracture toughness specimen.

V. CONCLUSIONS

A comprehensive examination of the 4.5-inch (114 mm) plate 7075-T7351 aluminum alloy intended for Shuttle applications reveals that:

- The material contains a number of macro- and microstructural inhomogeneities which could be classed as defects or potential crack-like defects, viz. stringers of brittle constituent particles, shrinkage cavities, and in one instance, a long line of spongelike porosity.

- Uniaxial strength level data obtained for the three primary orientations exceed design requirements for Shuttle application as well as procurement specifications.

- Similarly, results for cracking resistance - in terms of fracture toughness (K_{Ic}), fatigue crack growth rates (DA/DN), and rotating-beam fatigue life (S/N) appear to meet or exceed handbook levels.

- Unusual macroappearance of anodized components may be attributable to entrapment of anodizing solution by microshrinkage cavities and/or microcracks along constituent particle stringer interfaces, with subsequent seepage and staining adjacent to these and/or other flaws.

ACKNOWLEDGMENTS

The authors are grateful to Joel Berman, Martin Cigledy and Clark Welsh for their assistance with assorted experimental aspects of this work. Appreciation is offered to A. B. Jacoby, L. M. Turner and A. Harrison for their helpful discussions and guidance in the course of this work.

TABLE 1 - UNIAXIAL TENSILE PROPERTIES: 0.505 IN. DIA. SPECIMENS (Plate A)

ORIENTATION*	SPECIMEN NUMBER	0.2% OFFSET YIELD STRENGTH		ULTIMATE TENSILE STRENGTH		REDUCTION IN AREA	ELONGATION IN 2-IN. G.L.
		ksi	MPa	ksi	MPa	%	%
T (surface)	AT-1S	59.5	411	71.0	490	20	23
	AT-2S	54.9	379	66.7	460	14	20
	AT-3S	59.4	410	71.1	490	21	23
	Average	57.9	399	69.6	480	18	22
T (center)	AT-2C	55.5	383	66.6	459	18	21
	AT-3C	54.4	375	66.7	460	17	21
	Average	55.0	379	66.7	460	17	21
L (surface)	AL-1S	58.5	403	68.7	474	37	34
	AL-2S	58.3	402	68.7	474	47	34
	AL-3S	-	-	69.1	476	44	33
	Average	58.4	403	68.8	475	43	34
L (center)	AL-1C	60.2	415	71.9	496	31	26
	AL-2C	58.4	403	70.2	484	29	25
	Average	59.3	409	71.0	490	30	26

*T = long transverse, L = longitudinal

TABLE 2 - UNIAXIAL TENSILE PROPERTIES: 0.250 IN. DIA. SPECIMENS

ORIENTATION*	SPECIMEN NUMBER	0.2% OFFSET YIELD STRENGTH		ULTIMATE TENSILE STRENGTH		REDUCTION IN AREA	ELONGATION IN 1-IN. G.L.
		ksi	MPa	ksi	MPa	%	%
Plate A:							
S	AS-1	54.3	374	62.2	429	9	8
	AS-3	47.9	330	61.0	421	15	10
	AS-5	47.8	330	61.0	421	11	10
	Average	50.0	345	61.4	423	12	9
Plate A:							
T (surface)	ATT-1S	58.4	403	69.3	478	23	16
	ATT-2S	57.2	394	68.8	474	28	16
	ATT-3S	57.0	393	68.6	473	32	14
	Average	57.5	396	68.9	475	28	15
Plate B:							
S	BS-1	58.0	400	61.5	424	8	8
	BS-3	46.7	322	59.9	413	9	9
	Average	52.4	361	60.7	419	9	9

*S = short transverse, T = long transverse

TABLE 3 - PLANE STRAIN FRACTURE TOUGHNESS (K_{IC})

PLATE	ORIENTATION	SPECIMEN NUMBER	FRACTURE TOUGHNESS	
			ksi$\sqrt{in}$	MPa$\sqrt{m}$
A	LT (surface)	ALT-1S	(44.1)*	(48.5)*
		ALT-2S	(43.2)*	(47.5)*
		Average	(43.7)*	(48.0)*
A	LT (center)	ALT-1C	(40.3)*	(44.3)*
		ALT-2C	(41.0)*#	(45.1)*#
		Average	(40.7)*	(44.7)*
A	TL (surface)	ATL-1S	33.1	36.4
		ATL-2S	35.2	38.7
		Average	34.2	37.6
A	TL (center)	ATL-1C	34.0	37.4
		ATL-2C	33.4	36.7
		Average	33.7	37.0
A	ST	AST-1	>25.2	>27.7
		AST-2	(31.9)*	(35.1)*
		Average	(31.9)*	(35.1)*
B	ST	BST-1	26.7	29.3
		BST-2	28.2	31.0
		Average	27.5	30.2

*Invalid according to ASTM-E399-83, section 9.1.3: a, B $< 2.5 (K_Q/\sigma_{ys})^2$

#Invalid according to ASTM-E399-83, section 9.1.2: $P_{max}/P_Q > 1.10$

TABLE 4 - ROTATING BEAM FATIGUE LIFE: MAXIMUM STRESS = 40 ksi (276 MPa)

PLATE	ORIENTATION	SPECIMEN NO.	CYCLES TO FAILURE
A	L (surface)	ALR-4S	918,400
		ALR-5S	768,700
		ALR-6S	1,171,300
		Average	952,800
A	L (center)	ALR-4C	349,500
		ALR-5C	327,600
		ALR-6C	283,100
		Average	320,000
A	T (surface)	ATR-4S	1,253,600
		ATR-5S	1,045,900
		ATR-6S	1,062,500
		Average	1,120,667
A	T (center)	ATR-4C	312,500
		ATR-5C	290,500
		ATR-6C	310,800
		Average	304,600
A	S	ASR-4	123,200
		ASR-5	172,100
		ASR-6	159,800
		Average	155,033
B	S	BSR-4	175,100
		BSR-5	190,100
		BSR-6	158,400
		Average	174,533

TABLE 5 - ROTATING BEAM FATIGUE LIFE: MAXIMUM STRESS = 50 ksi (345 MPa)

PLATE	ORIENTATION	SPECIMEN NO.	CYCLES TO FAILURE
A	L (surface)	ALR-1S	196,600
		ALR-2S	254,300
		ALR-3S	233,900
		Average	228,267
A	L (center)	ALR-1C	190,500
		ALR-2C	152,000
		ALR-3C	88,500
		Average	143,667
A	T (surface)	ATR-3S	248,600
		Average	248,600
A	T (center)	ATR-1C	70,600
		ATR-2C	79,500
		ATR-3C	66,400
		Average	72,167
A	S	ASR-1	47,800
		ASR-2	49,700
		ASR-3	53,200
		Average	50,233
B	S	BSR-1	59,200
		BSR-2	44,900
		BSR-3	38,900
		Average	47,667

Fig. 1 - Dye penetrant appearance of plate section as observed with ultraviolet light.

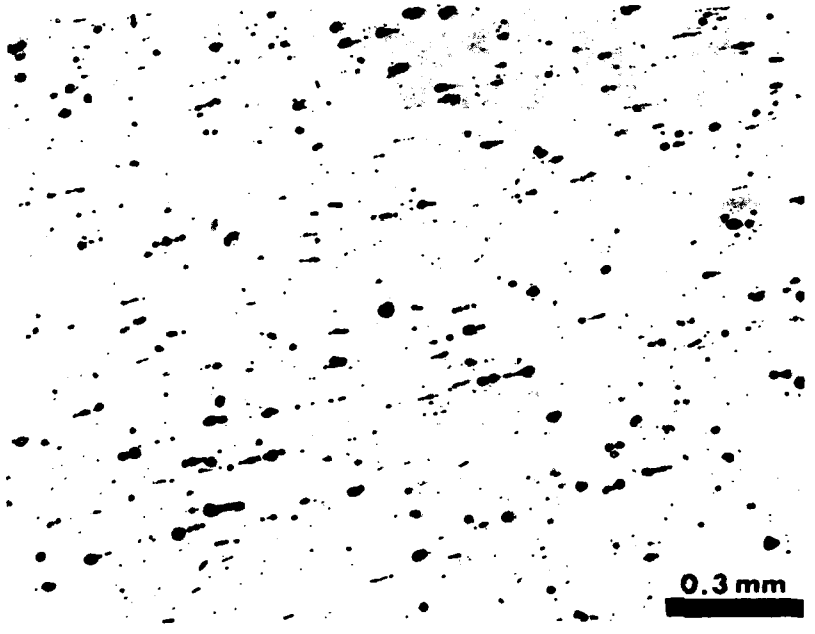

Fig. 2 - Constituent particles at plate surface location, as polished, T-orientation.

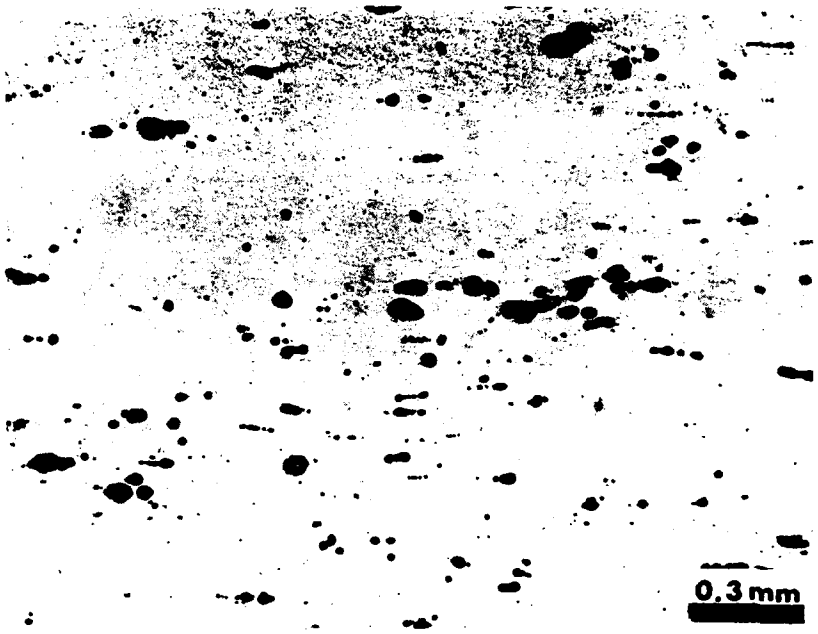

(a)

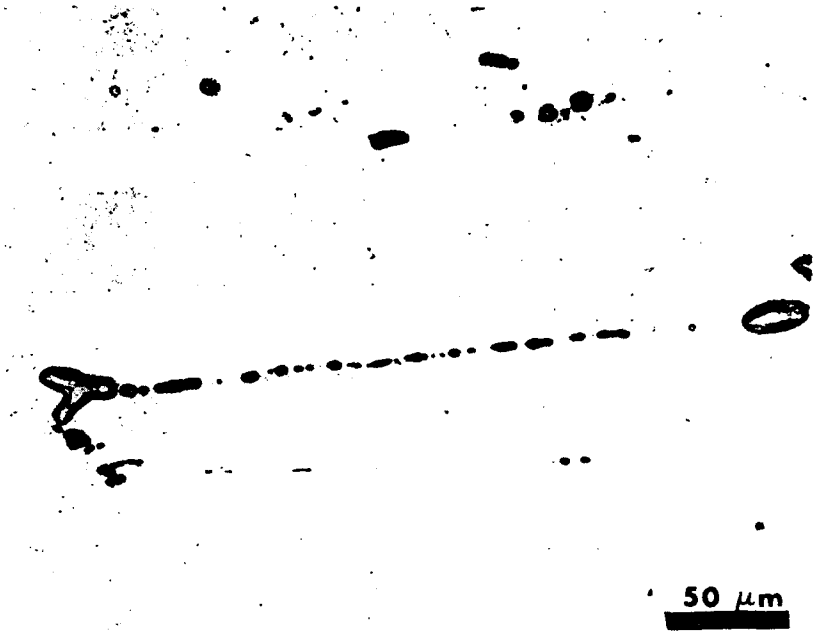

(b)

Fig. 3 - Constituent particles at plate midthickness location, as polished, T-orientation; (a) overall view (b) enlargement of sizeable stringer.

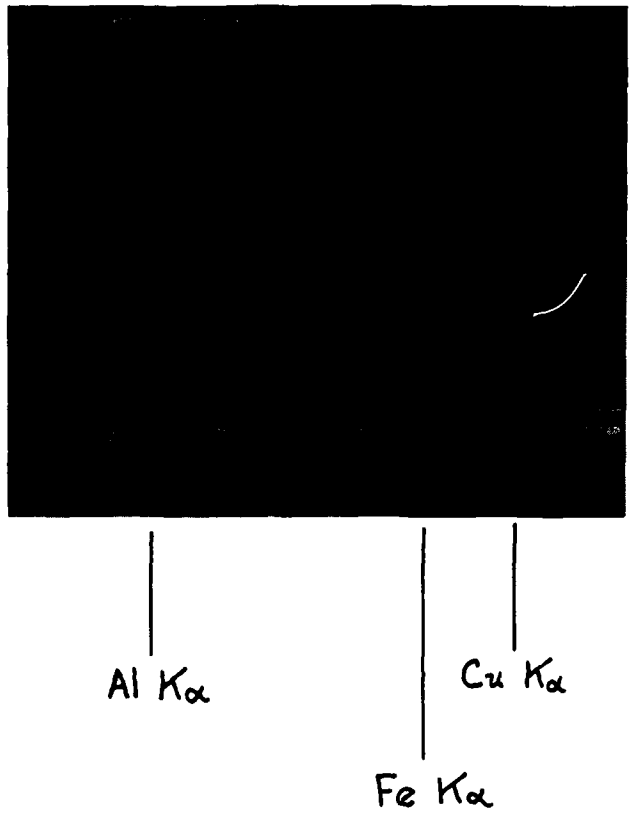

Fig. 4 - Electron probe X-ray microanalysis of dominant species of constituent particle.

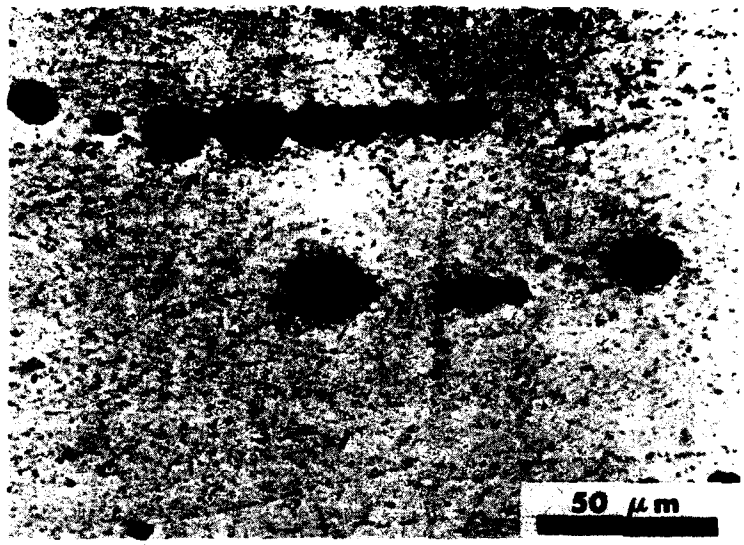

Fig. 5 - Enlarged view of constituent particles, after conventional vibratory (automated) polishing.

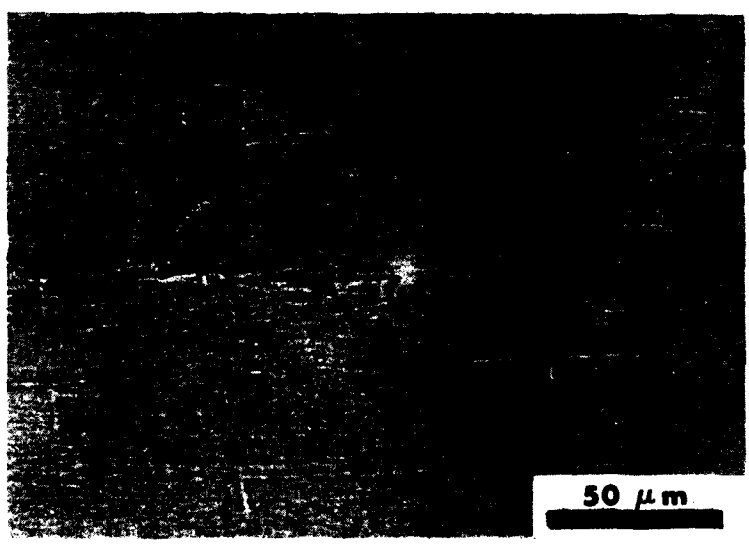

Fig. 6 - Enlarged view of constituent particles, after hand polishing very carefully with diamond paste.

Fig. 7 - Large shrinkage cavity at plate midthickness location, as polished.

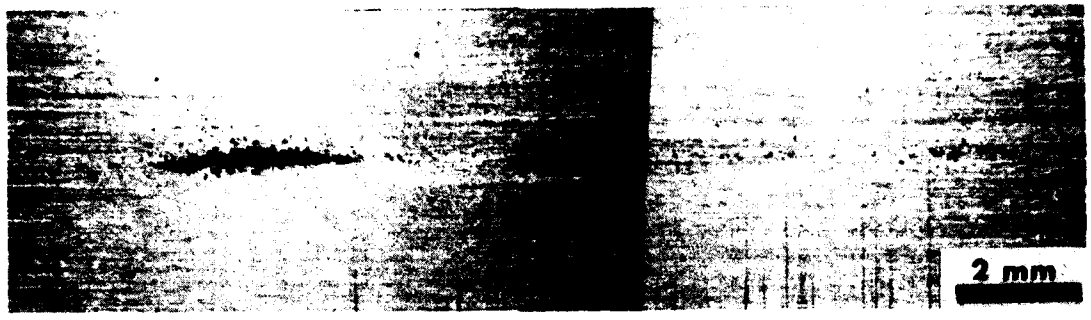

(a)

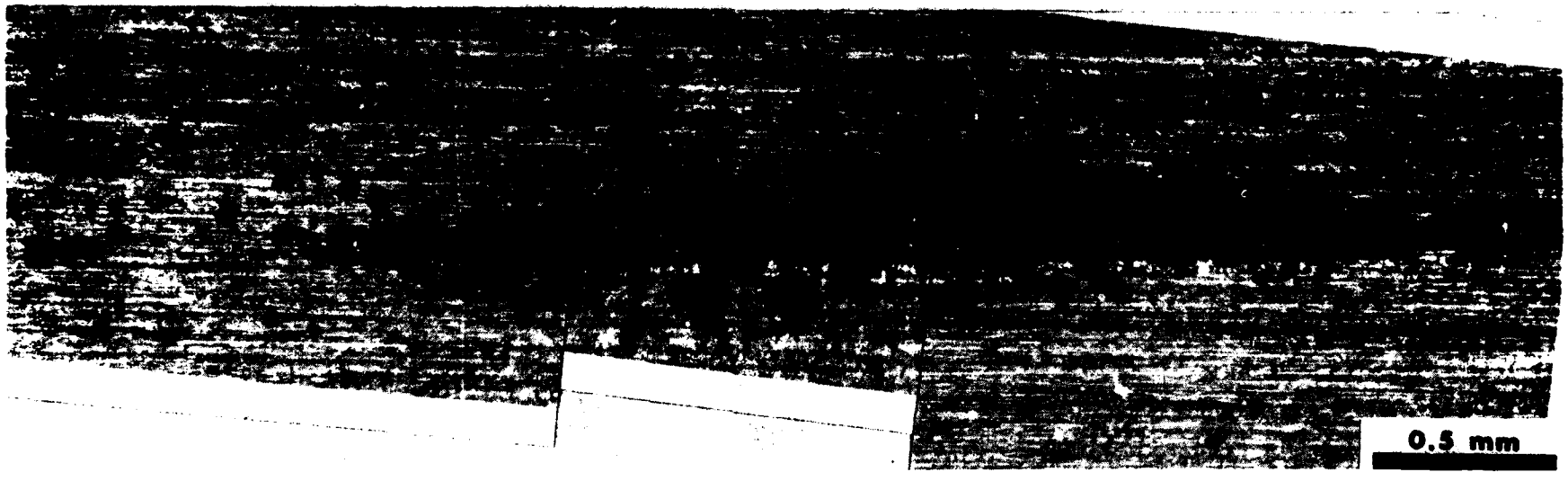

(b)

Fig. 8 - Long narrow band (S-orientation), of spongelike porosity as rough polished. (a) overall view (b) enlargement.

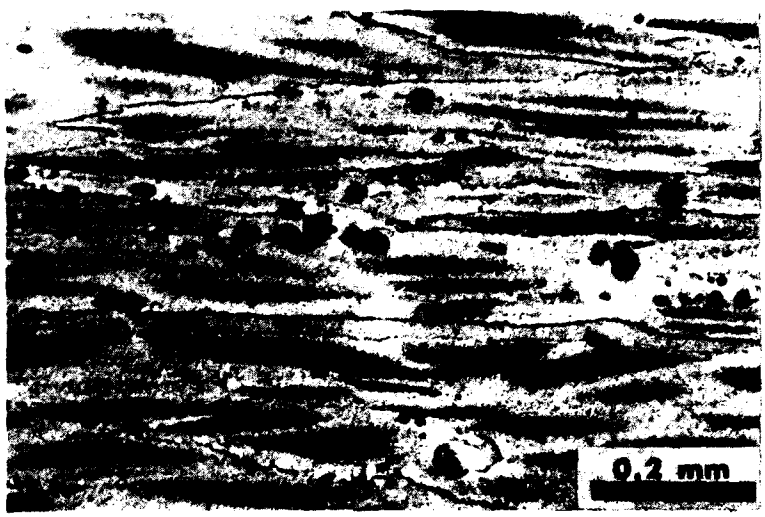

Fig. 9 - Microstructure as etched with Keller's reagent, plate midthickness location, T-orientation.

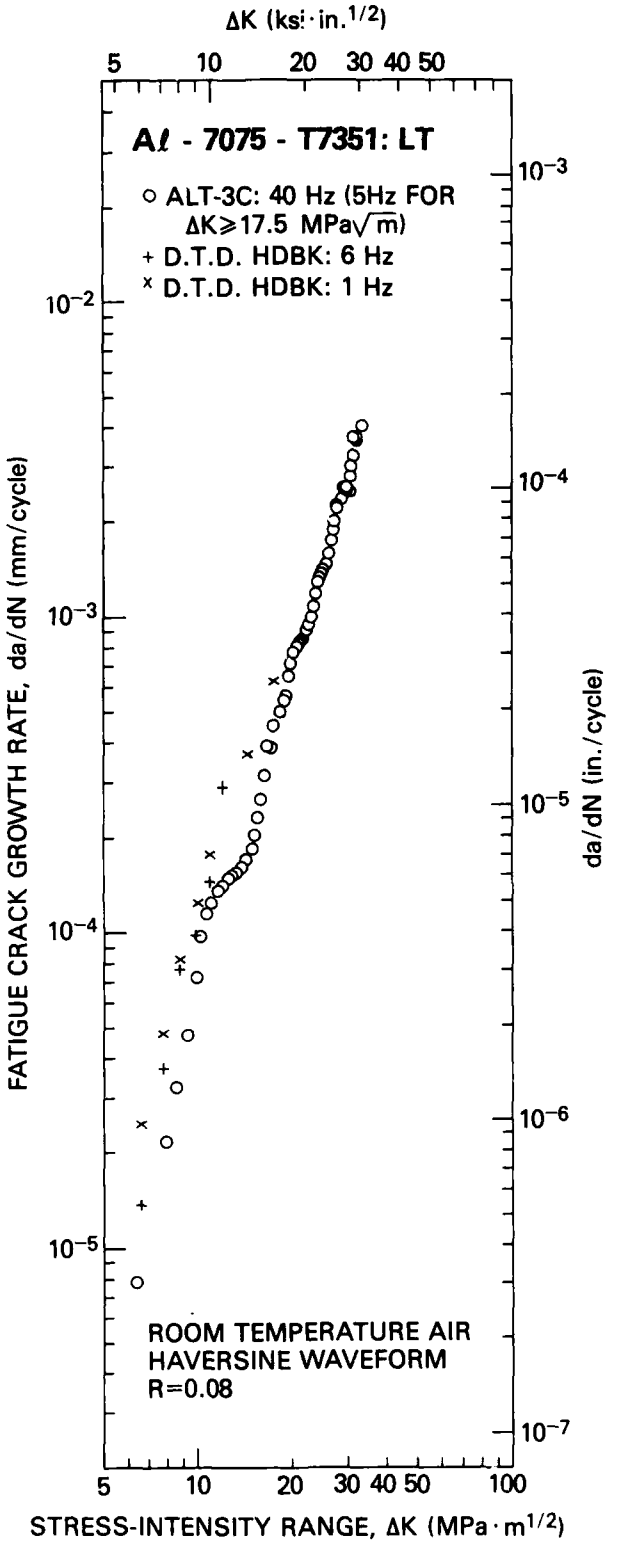

Fig. 10 - Fatigue crack growth rates for LT orientation at plate midthickness location (specimen no. ALT-3C), with comparison to handbook data from reference [9].

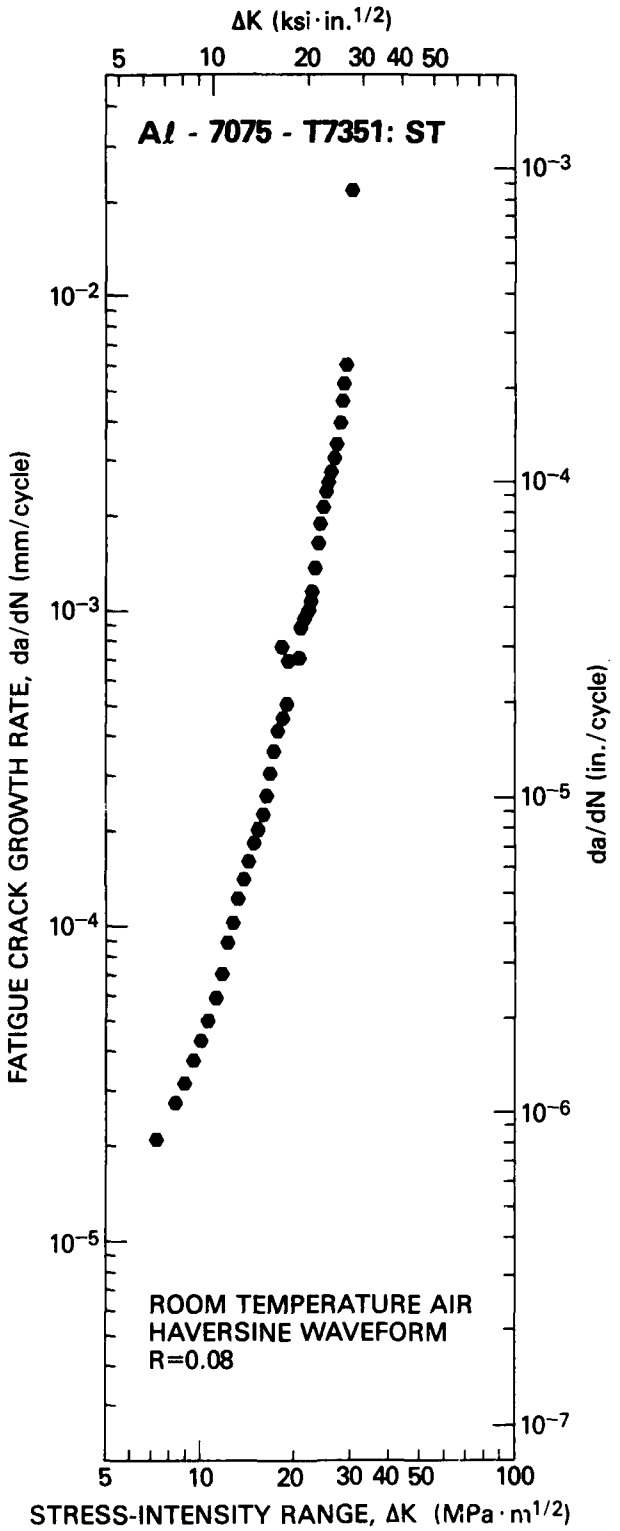

Fig. 11 - Fatigue crack growth rates for ST orientation (specimen no. AST-3).

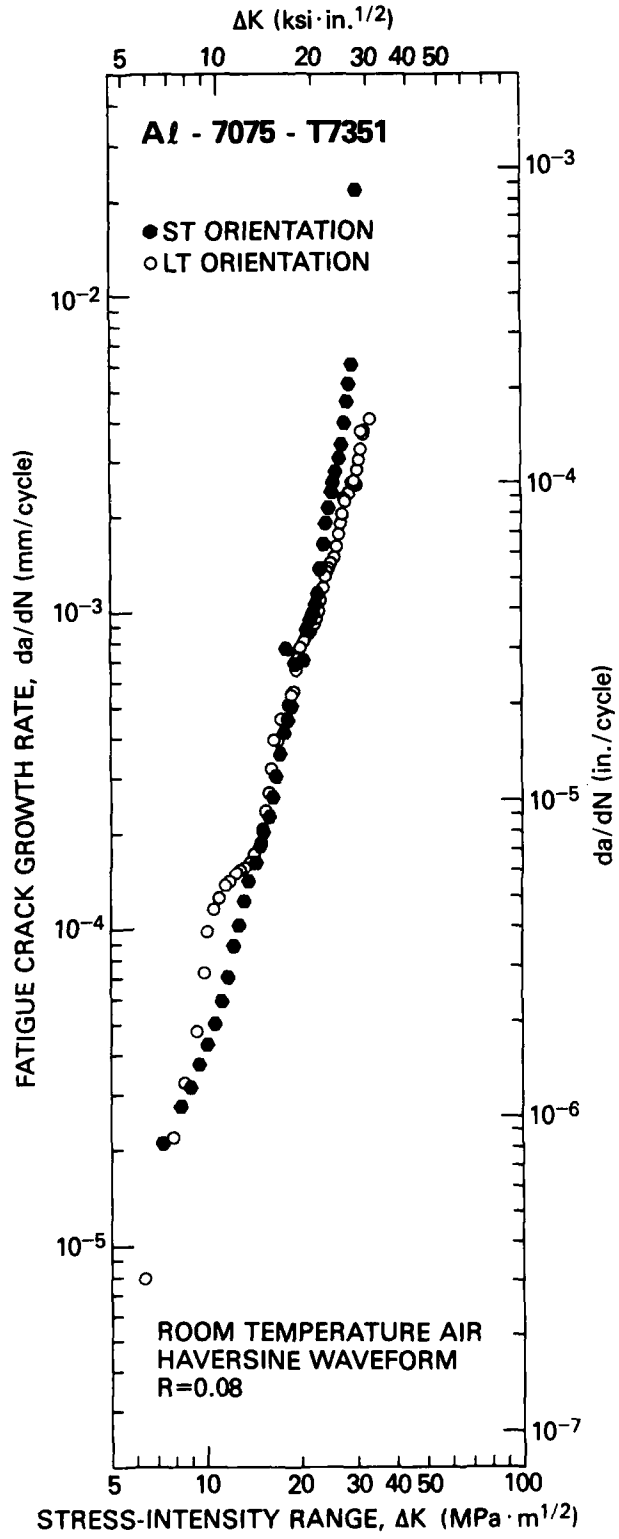

Fig. 12 - Comparison of fatigue crack growth rates for LT and ST orientations in 4.5 inch plate material.

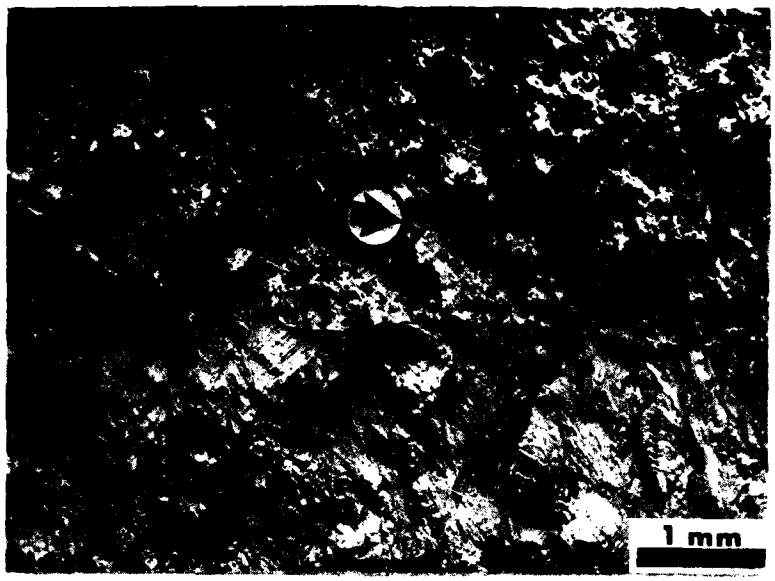

Fig. 13 - Scanning electron micrograph of fracture toughness specimen of LT orientation with fatigue precrack zone in lower half; direction of crack growth is from bottom to top. Arrow points to secondary crack along S-plane in fracture process zone.

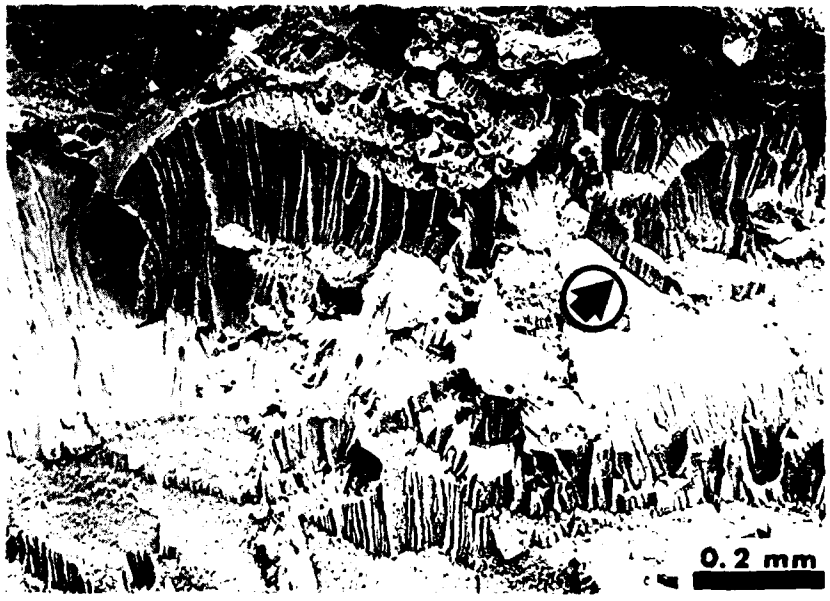

Fig. 14 - Scanning electron micrograph of crystallographic bifurcation in fatigue precrack zone of fracture toughness specimen of ST orientation (spec. no. AST-1); arrow points to secondary crack. Direction of crack growth is from bottom to top, with fracture process zone at top edge of micrograph.

REFERENCES

[1] T. H. Sanders, Jr., R. R. Sawtell, J. T. Staley, R. J. Bucci and A. B. Thakker: "Effect of Microstructure on Fatigue Crack Growth of 7XXX Aluminum Alloys Under Constant Amplitude and Spectrum Loading," Final Report No. 56-78-AF8, Aluminum Company of America, Alcoa Center, PA, 14 April 1978.

[2] F. Keller and G. W. Wilcox: "Identification of Constituents of Aluminum Alloys," *Technical Paper* No. 7, Aluminum Company of America, Alcoa Center, PA, 1942.

[3] "Cleaning and Finishing of Aluminum and Aluminum Alloys," ASM Metals Handbook, Eighth Edition, Vol. 2, Taylor Lyman, Editor, American Society for Metals, Metals Park, OH, 1964, pp. 611-634.

[4] Eugene Smith, Naval Research Laboratory, Washington, DC, personal communication, 16 July 1985.

[5] ASTM E8-83, "Standard Methods of Tension Testing of Metallic Materials," Annual Book of ASTM Standards, Vol. 03.01. Sec. 3, American Society for Testing and Materials, Philadelphia, PA, 1984, pp. 130-150.

[6] ASTM E399-83, "Standard Test Method for Plane-Strain Fracture Toughness of Metallic Materials," Annual Book of ASTM Standards, Vol. 03.01, Sec. 3, American Society for Testing and Materials, Philadelphia, PA, 1984, pp. 519-554.

[7] ASTM E647-83, "Standard Test Method for Constant-Load-Amplitude Fatigue Crack Growth Rates Above 10^{-8} m/Cycle," Annual Book of ASTM Standards, Vol. 03.01, Sec. 3, American Society for Testing and Materials, Philadelphia, PA, 1984, pp. 711-731.

[8] G. R. Yoder, L. A. Cooley and T. W. Crooker: "Procedures for Precision Measurement of Fatigue Crack Growth Rate Using Crack-Opening Displacement Techniques," Fatigue Crack Growth Measurement and Data Analysis, ASTM STP 738, S. J. Hudak, Jr. and R. J. Bucci, Editors, American Society for Testing and Materials, Philadelphia, PA, 1981, pp. 85-102.

[9] "7000 Aluminum Alloy," Damage Tolerant Design Handbook, J. P. Gallagher, Editor, Vol, 3, Chapter 8, Metals and Ceramics Information Center, Battelle-Columbus Laboratories, Columbus, Ohio, December 1983, pp. 8.0-3 - 8.8-13.

[10] T. W. Crooker: "Fracture Mechanics Fatigue Design," Mechanical Engineering, Vol. 99, No. 6, 1977, pp. 40-45.

[11] R. W. Hertzberg: Deformation and Fracture Mechanics of Engineering Materials, Second Edition, John Wiley & Sons, New York, 1983, pp. 541-548.

[12] "7075 Al," Aerospace Structural Metals Handbook, Vol. 3, Code 3207 Mechanical Properties Data Center, Battelle's Columbus Laboratories, Columbus, OH, 1982, pp. 1-32.

[13] G. R. Yoder, L. A. Cooley and T. W. Crooker: "On the Role of Microstructure in the Growth of Fatigue Cracks," Fatigue 84 (Proceedings of the Second International Conference on Fatigue and Fatigue Thresholds, University of Birmingham, United Kingdom, 3-7 September 1984), Vol. 1, C. J. Beevers, Editor, EMAS, Ltd., West Midlands, U.K., 1984, pp. 351-360.

[14] G. R. Yoder, L. A. Cooley and T. W. Crooker: "On Microstructural Control of Near-Threshold Fatigue Crack Growth in 7000-Series Aluminum Alloys," Scripta Metallurgica, Vol. 16, No. 9, 1982, pp. 1021-1025.

[15] G. R. Yoder, L. A. Cooley and T. W. Crooker: "Quantitative Analysis of Microstructural Effects on Fatigue Crack Growth in Widmanstätten Ti-6Al-4V and Ti-8Al-1Mo-1V," Engineering Fracture Mechanics, Vol. 11, 1979, pp. 805-816.

APPENDIX A

LOAD-DISPLACEMENT RECORDS

This appendix contains records of crack-mouth-opening-displacement (CMOD) as a function of applied load, as relate to the plane strain fracture toughness (K_{Ic}) results given in Table 3.

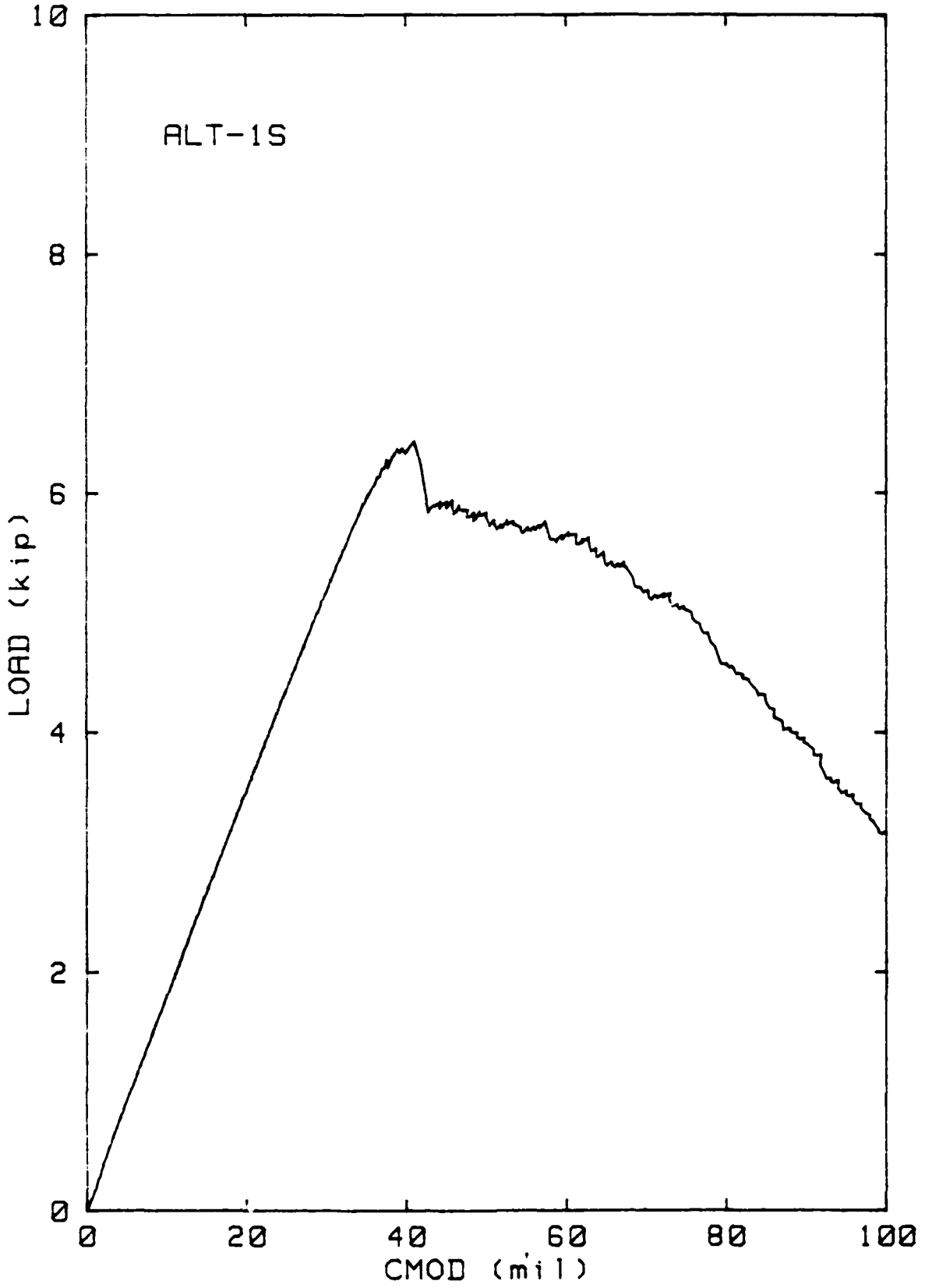
ALT-1S
LOAD (kip)
CMOD (mil)
0
2
4
6
8
10
0
20
40
60
80
100

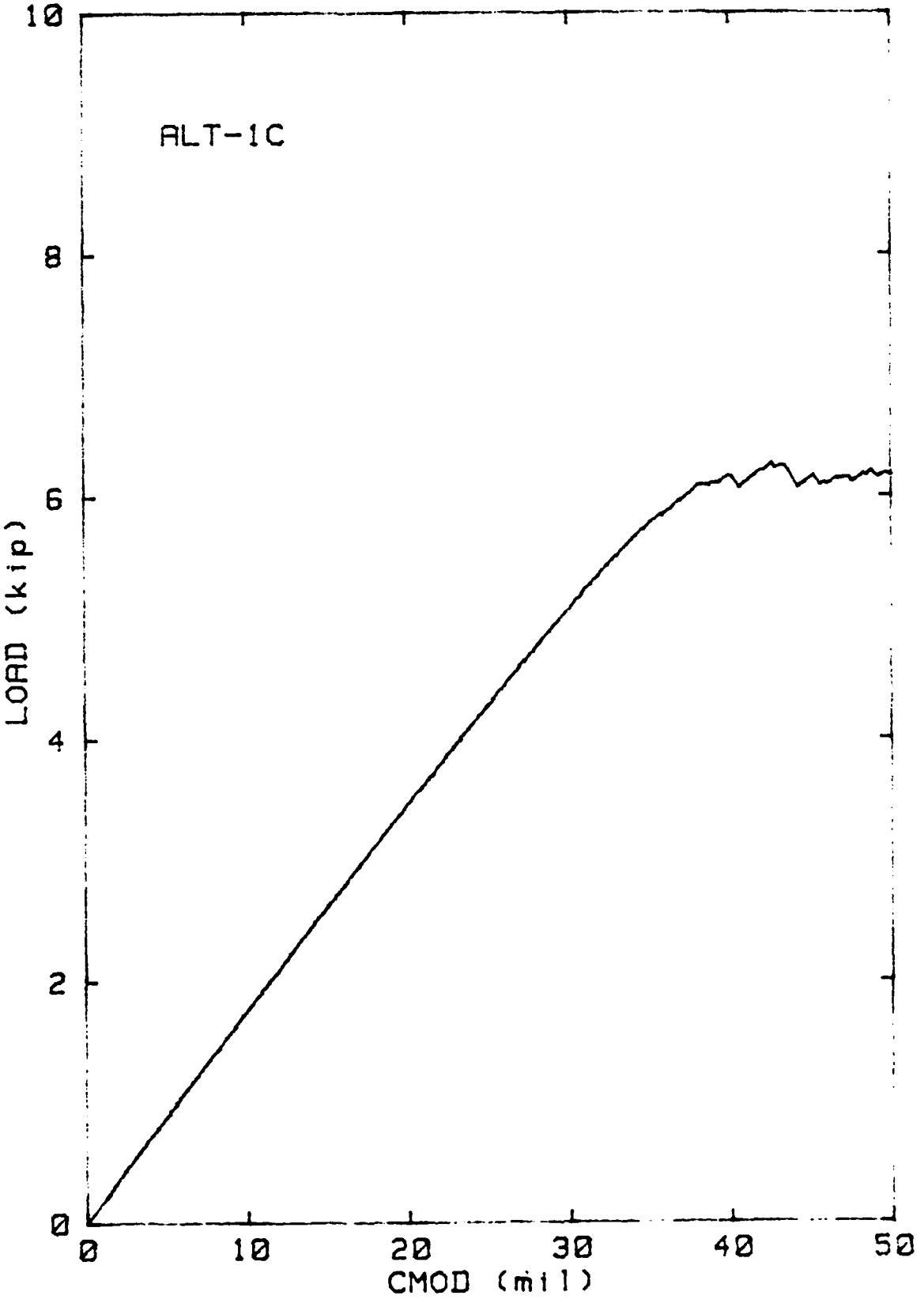
ALT-1C
LOAD (kip)
CMOD (mil)
0
2
4
6
8
10
0
10
20
30
40
50

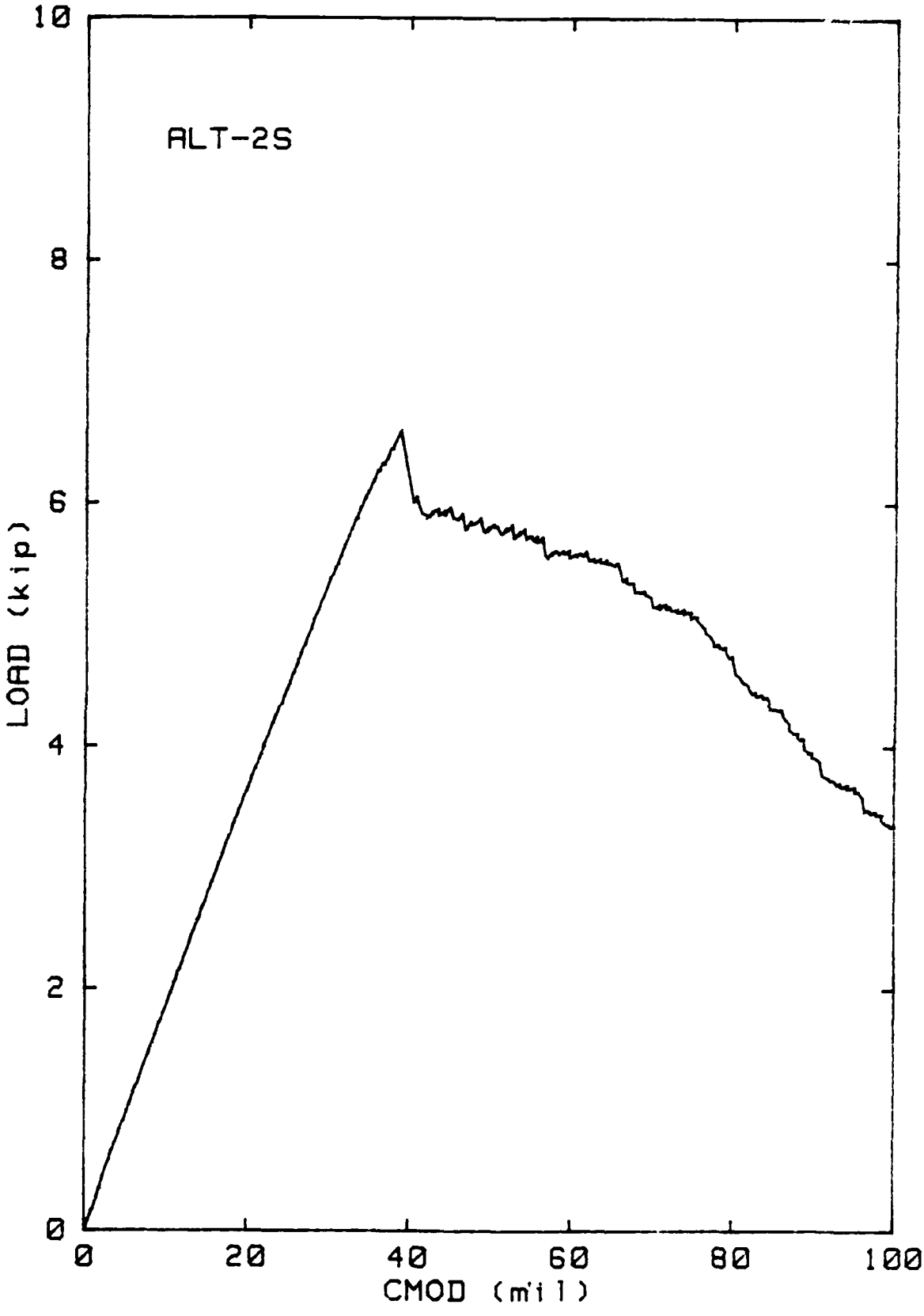
ALT-2S
LOAD (kip)
CMOD (mil)
0
2
4
6
8
10
0
20
40
60
80
100

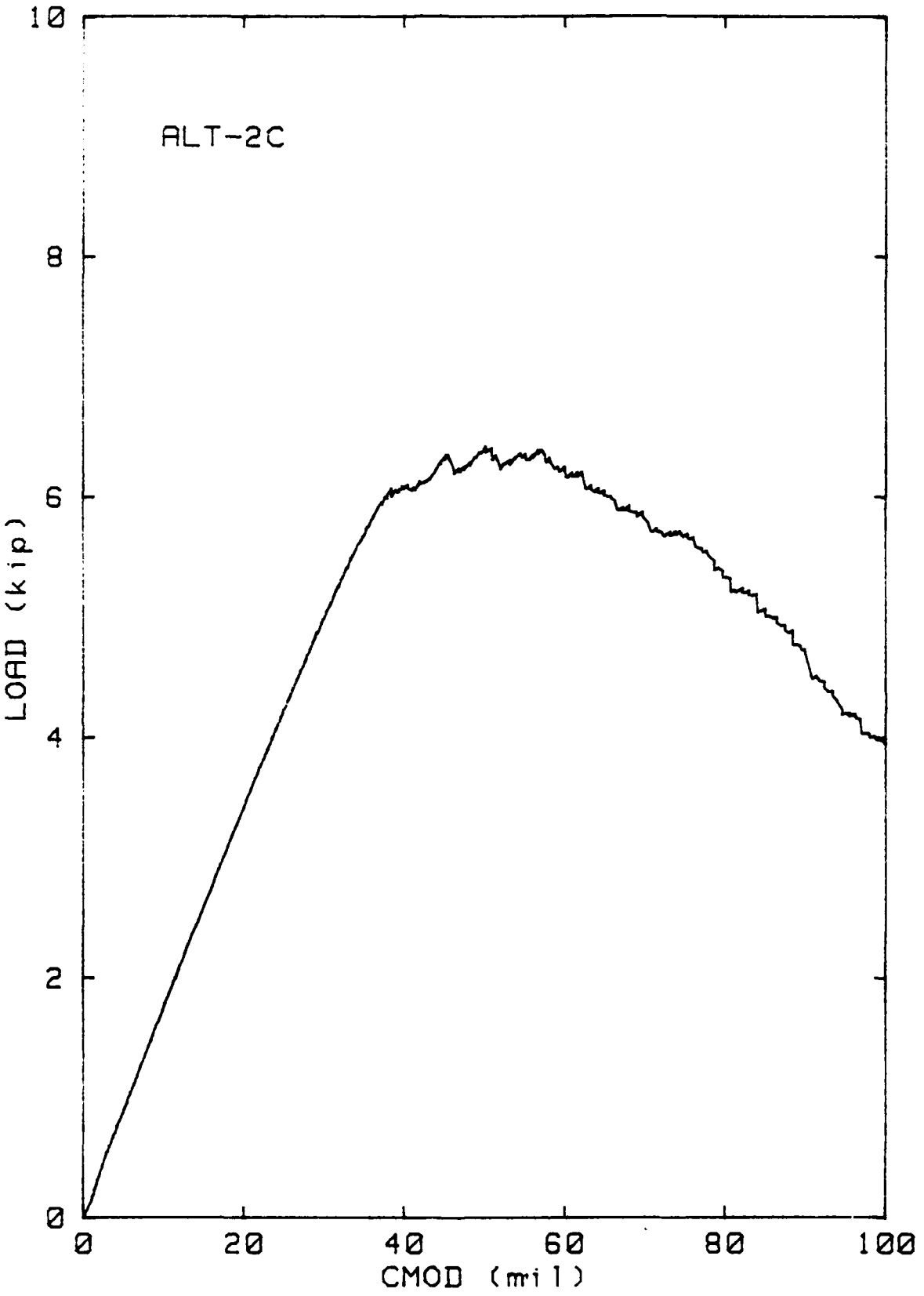
ALT-2C
LOAD (kip)
CMOD (mil)
0
2
4
6
8
10
0
20
40
60
80
100

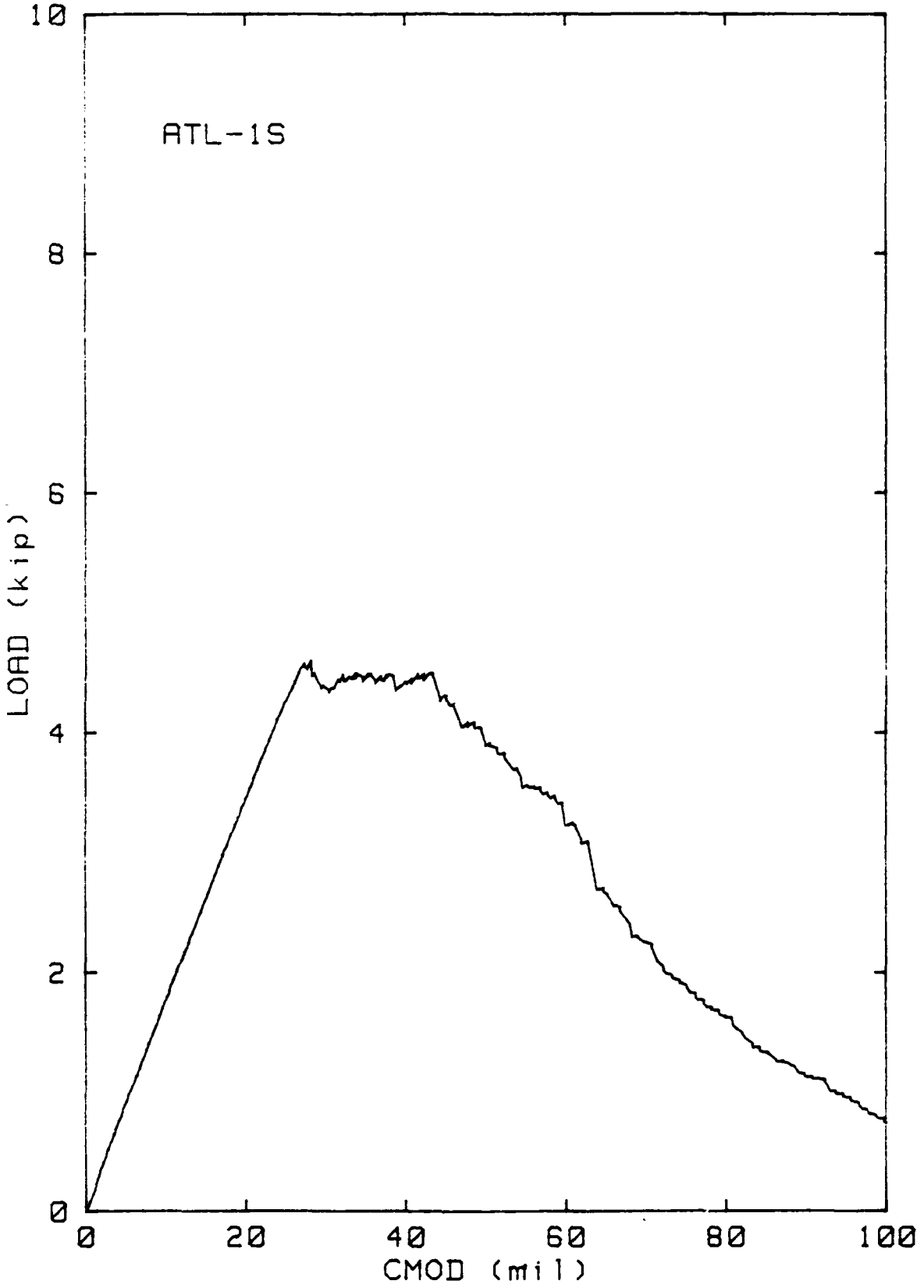
ATL-1S
LOAD (kip)
CMOD (mil)
0
2
4
6
8
10
0
20
40
60
80
100

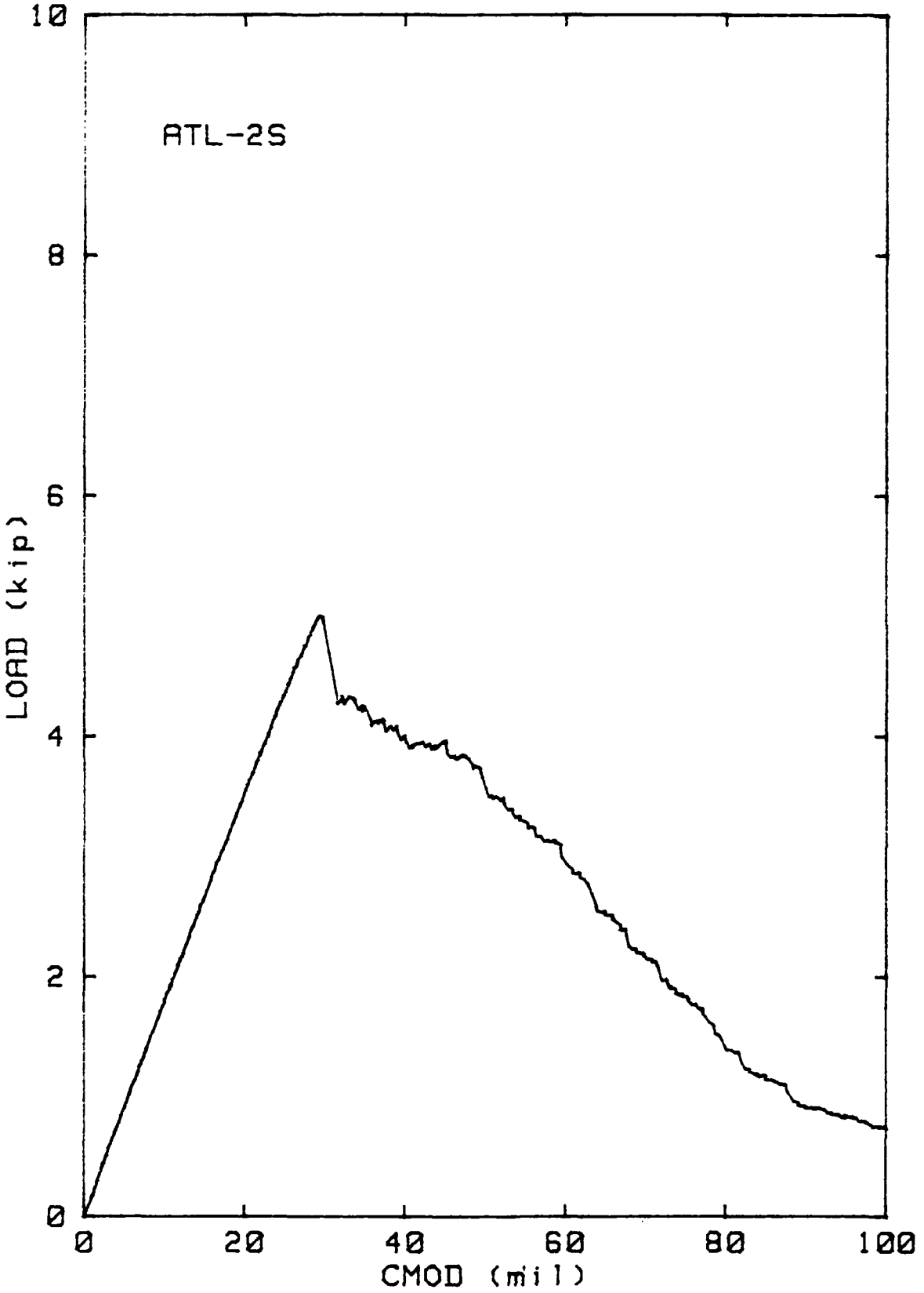
ATL-2S
LOAD (kip)
CMOD (mil)
0
2
4
6
8
10
0
20
40
60
80
100

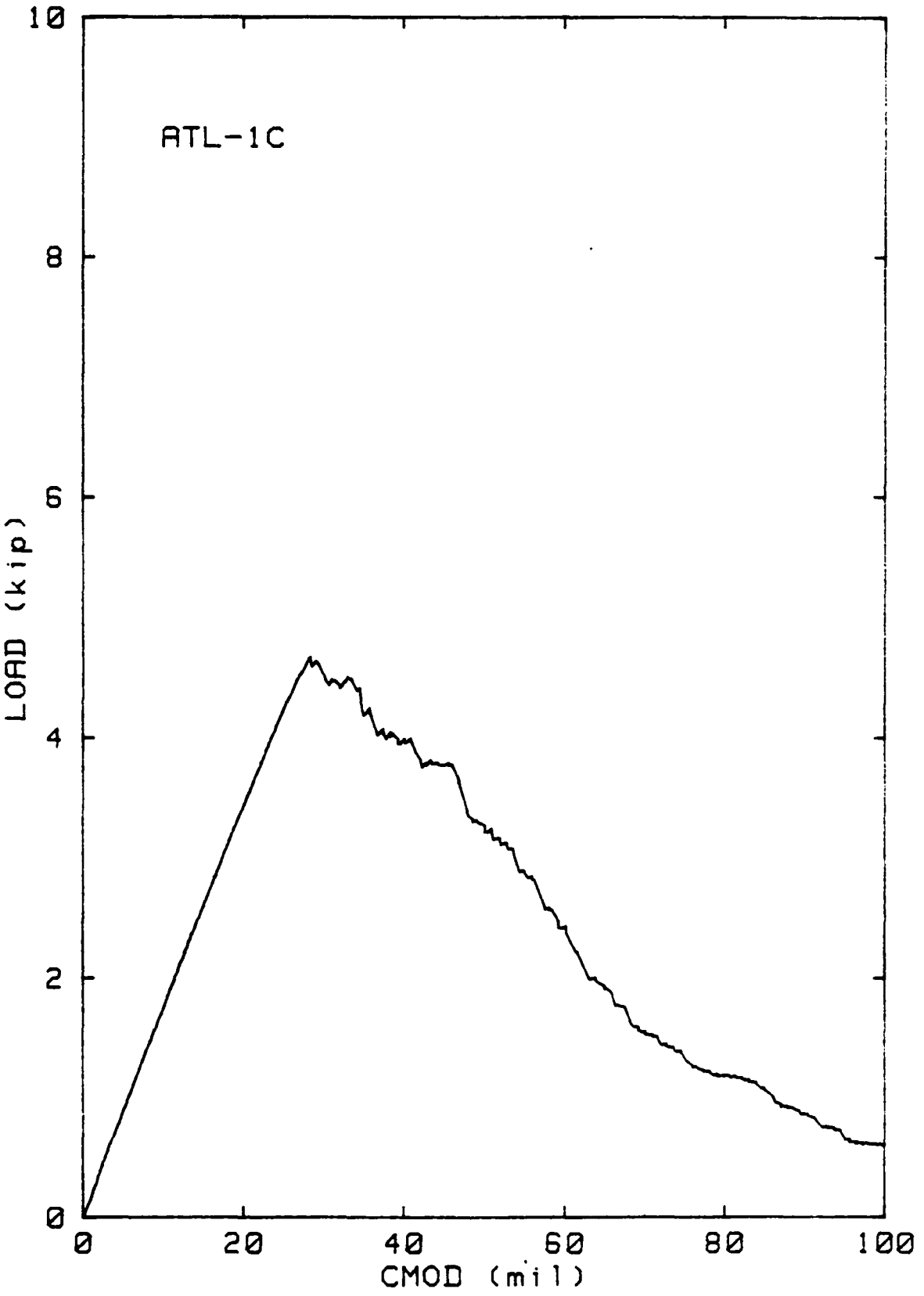
ATL-1C
LOAD (kip)
CMOD (mil)
0
2
4
6
8
10
0
20
40
60
80
100

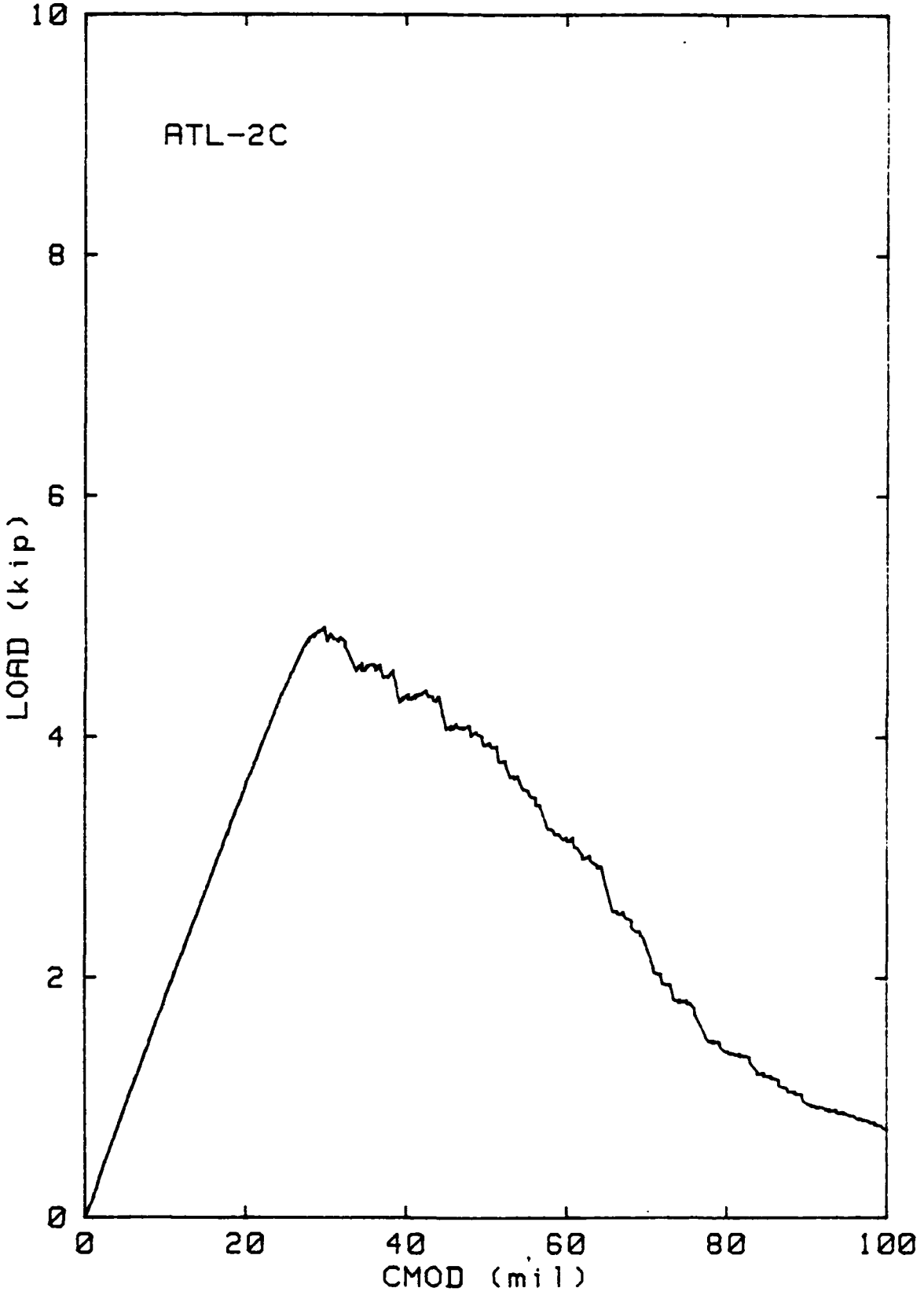
ATL-2C
LOAD (kip)
CMOD (mil)
0
2
4
6
8
10
0
20
40
60
80
100

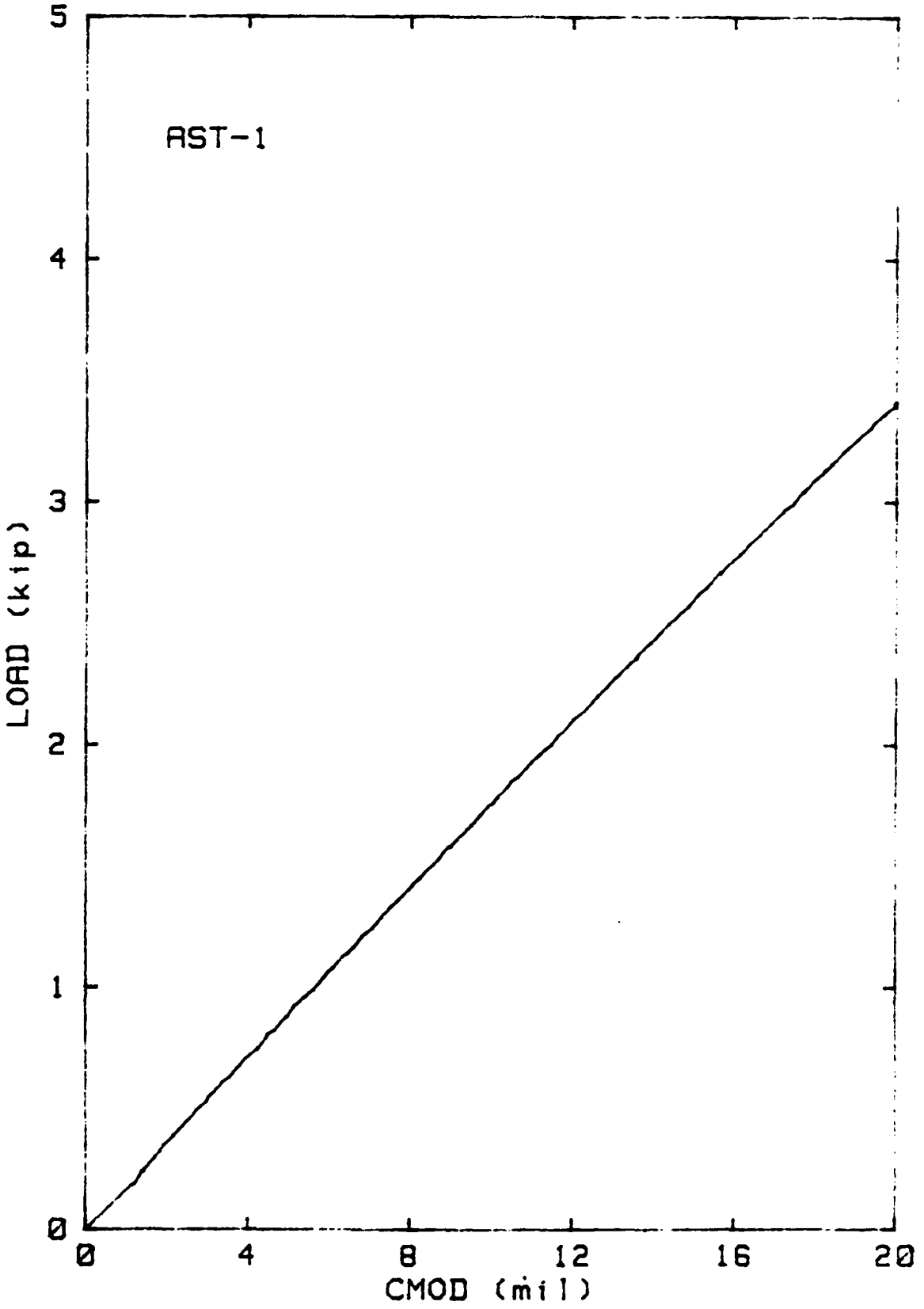
AST-1
LOAD (kip)
CMOD (mil)
0
1
2
3
4
5
0
4
8
12
16
20

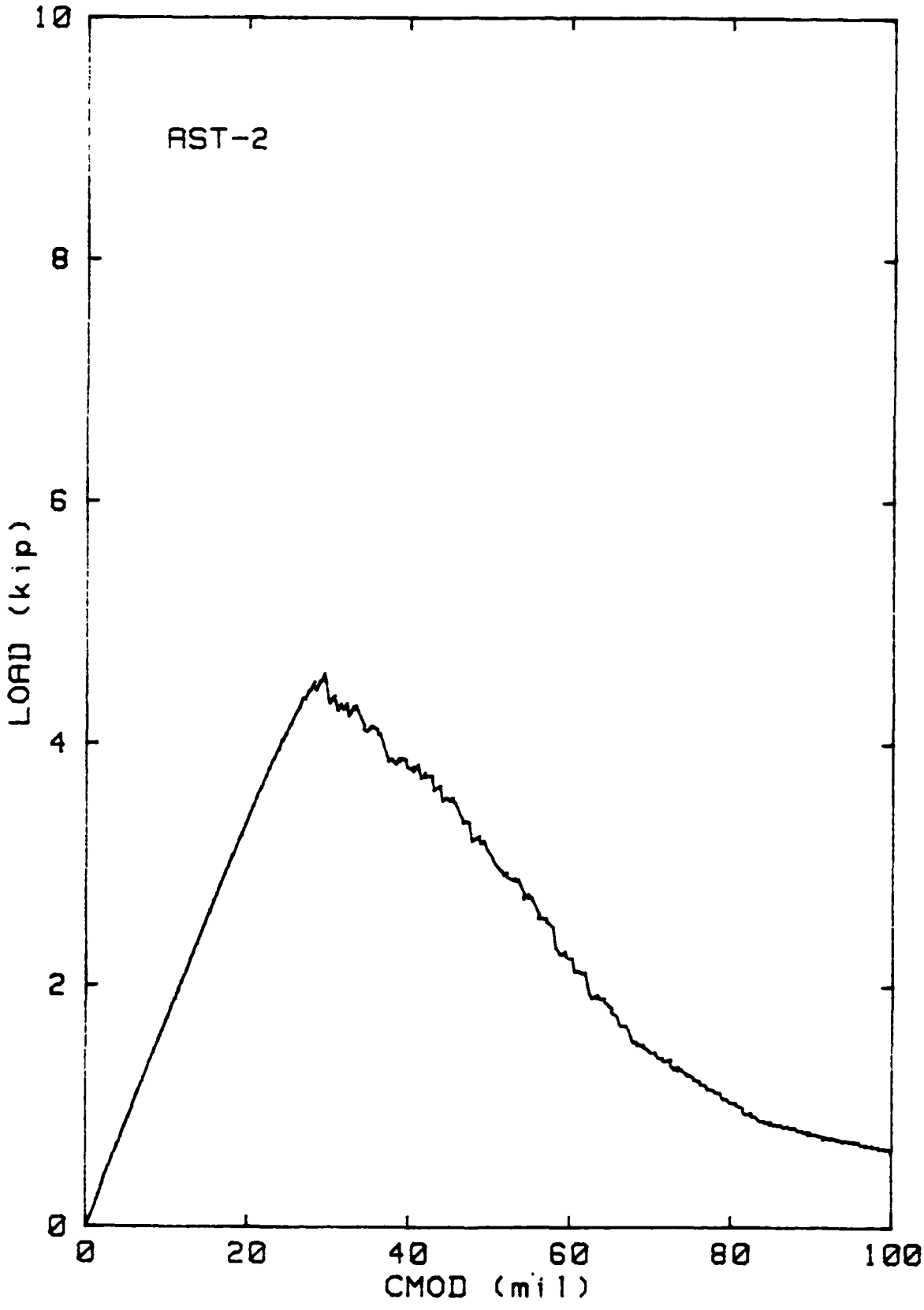
AST-2
LOAD (kip)
CMOD (mil)
0
2
4
6
8
10
0
20
40
60
80
100

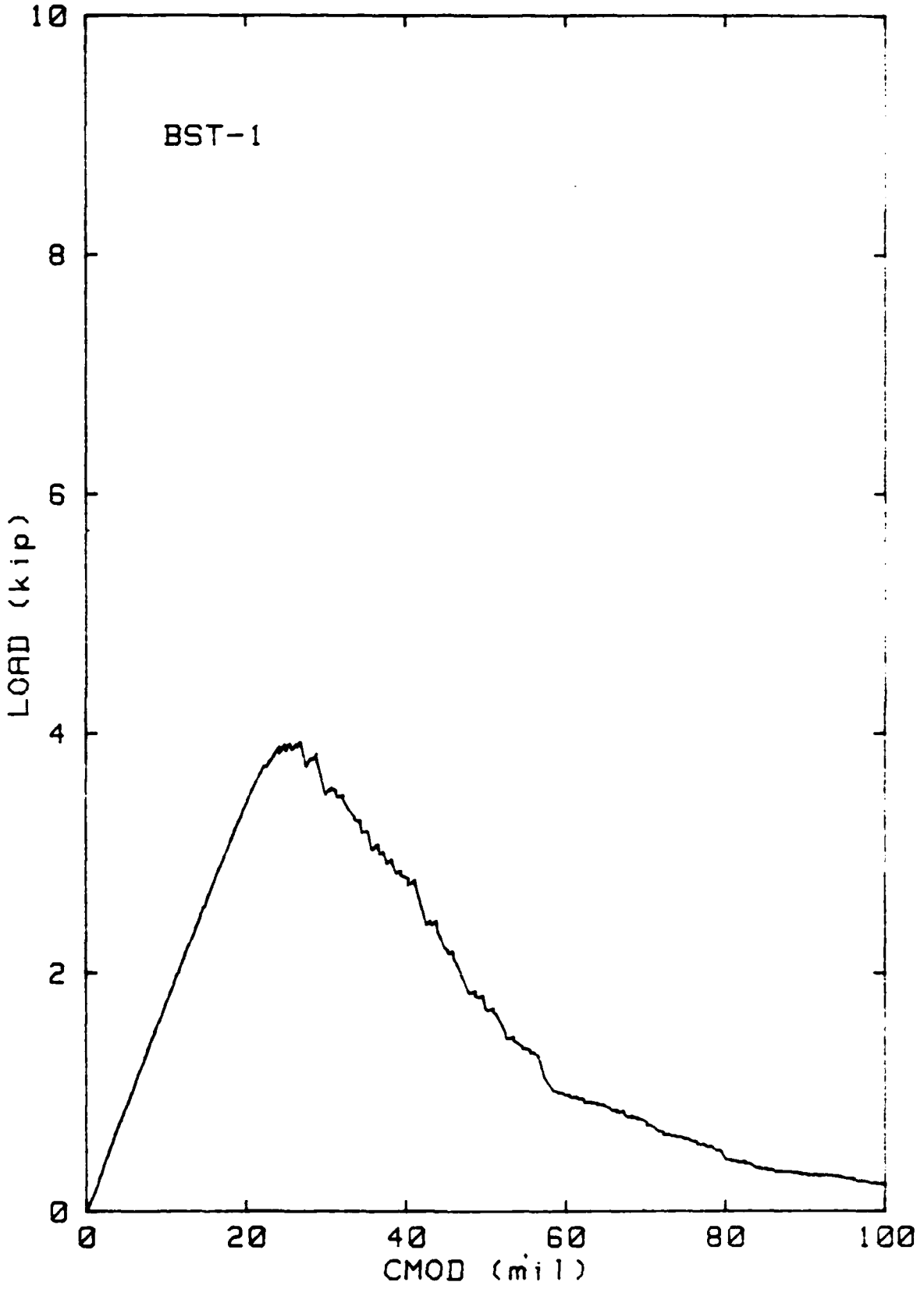
BST-1
LOAD (kip)
CMOD (mil)
0
2
4
6
8
10
0
20
40
60
80
100

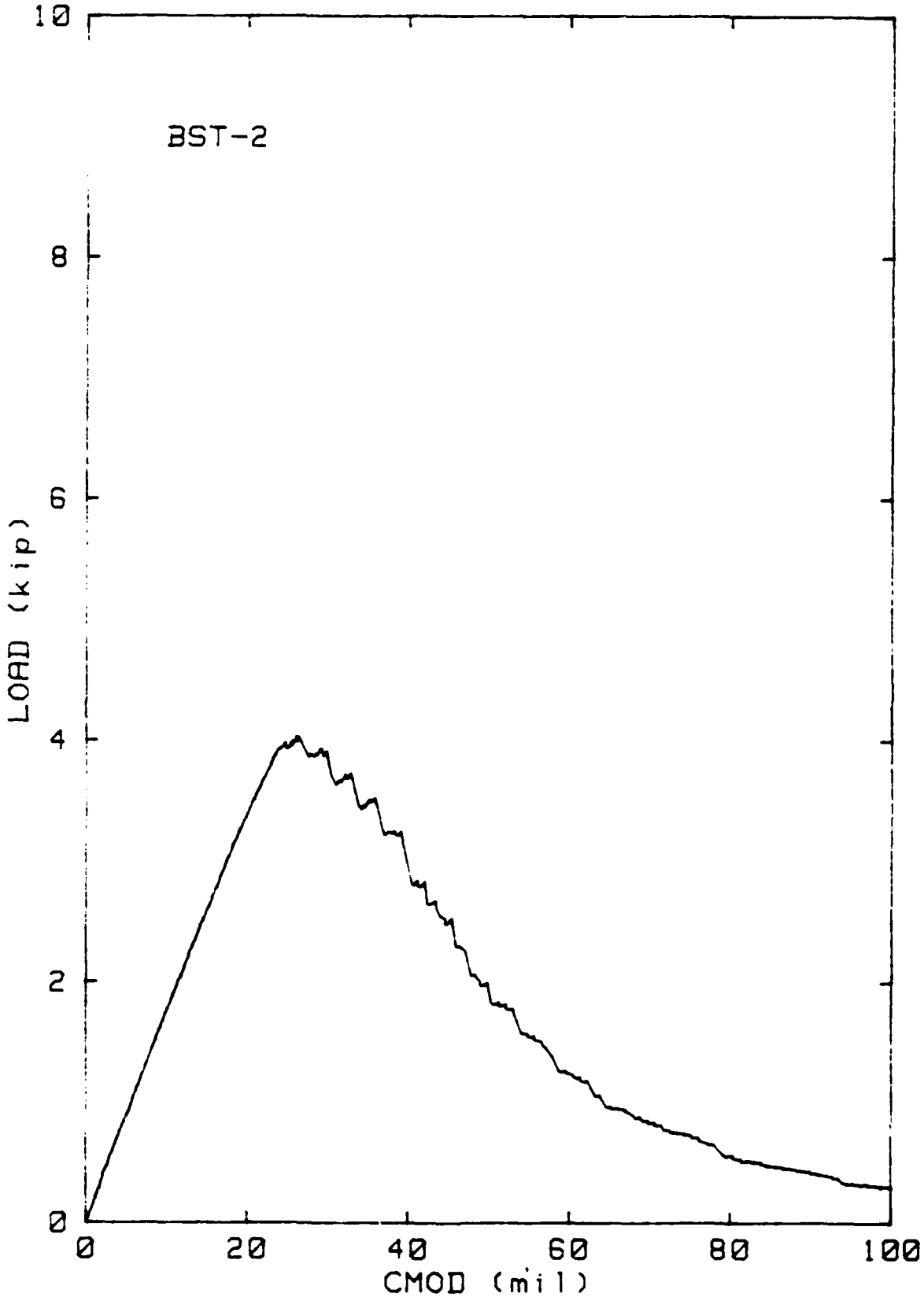
BST-2
LOAD (kip)
CMOD (mil)
10
8
6
4
2
0
0
20
40
60
80
100

APPENDIX B

FATIGUE CRACK PROPAGATION DATA

This appendix contains a tabulation of data for fatigue crack growth rate (DA/DN) as a function of stress-intensity range (ΔK) as plotted in Figs. 10-12 for specimens numbers ALT-3C (LT orientations) and AST-3 (ST orientation)

Specimen No. ALT-3C			
ΔK		da/dN	
MPa√m	ksi √in.	mm/cycle	in./cycle
6.40	5.82	7.88×10^{-5}	3.10×10^{-7}
7.85	7.14	2.20×10^{-5}	8.66
8.54	7.77	3.31	1.30×10^{-6}
9.33	8.49	4.80	1.89
9.89	9.00	7.37	2.90
10.18	9.26	9.87	3.89
10.62	9.66	1.16×10^{-4}	4.57
11.09	10.09	1.26	4.96
11.58	10.54	1.38	5.43
12.07	10.98	1.44	5.67
12.53	11.40	1.50	5.91
12.92	11.76	1.53	6.02
13.33	12.13	1.57	6.18
13.78	12.54	1.65	6.50
14.17	12.90	1.74	6.85
14.63	13.31	1.88	7.40
15.04	13.69	2.08	8.19
15.48	14.09	2.36	9.29
15.87	14.44	2.70	1.06×10^{-5}
16.28	14.82	3.22	1.27
16.65	15.15	3.96	1.56
17.18	15.63	3.94	1.55
17.46	15.89	4.61	1.82
18.00	16.38	4.65	1.83
18.37	16.72	5.10	2.01
18.80	17.11	5.52	2.17
19.24	17.51	5.65	2.22
20.18	18.36	7.81	3.07
20.55	18.70	8.20	3.23
20.95	19.06	8.41	3.31
21.33	19.41	8.57	3.37
21.68	19.73	8.78	3.46
22.05	20.07	9.13	3.59
22.45	20.43	9.61	3.78
22.85	20.79	1.02×10^{-3}	4.02
23.26	21.17	1.10	4.33
23.62	21.50	1.21	4.76
24.00	21.84	1.31	5.16
24.36	22.17	1.37	5.39
24.73	22.50	1.41	5.55
25.07	22.82	1.45	5.71
25.41	23.12	1.46	5.75
25.80	23.48	1.51	5.94
26.21	23.85	1.63	6.42
26.60	24.21	1.78	7.01
27.02	24.59	1.91	7.52
27.39	24.93	2.06	8.11
27.79	25.29	2.26	8.90
28.15	25.62	2.33	9.17
28.53	25.96	2.38	9.37
28.92	26.32	2.52	9.92
29.33	26.69	2.49	9.80
29.69	27.02	2.49	9.80
29.97	27.27	2.62	1.03×10^{-4}
30.56	27.81	2.83	1.11
30.91	28.13	3.07	1.21
31.27	28.46	3.30	1.30
31.65	28.80	3.74	1.47
32.07	29.18	3.66	1.44
32.53	29.60	3.80	1.50
33.53	30.51	4.10	1.61

Specimen No. AST-3			
ΔK		da/dN	
MPa√m	ksi √in.	mm/cycle	in./cycle
7.30	6.64	2.11×10^{-5}	8.31×10^{-7}
8.36	7.61	2.75	1.08×10^{-6}
8.94	8.14	3.19	1.26
9.53	8.67	3.74	1.47
10.12	9.21	4.31	1.70
10.64	9.68	5.04	1.98
11.20	10.19	5.91	2.33
11.69	10.64	7.12	2.80
12.24	11.14	8.90	3.50
12.66	11.52	1.03×10^{-4}	4.06
13.13	11.95	1.23	4.84
13.58	12.36	1.42	5.59
14.07	12.80	1.62	6.38
14.59	13.28	1.84	7.24
15.12	13.76	2.01	7.91
15.75	14.33	2.26	8.90
16.30	14.83	2.59	1.02×10^{-5}
16.82	15.31	3.02	1.19
17.33	15.77	3.57	1.41
17.80	16.20	4.19	1.65
18.19	16.55	4.61	1.81
18.52	17.13	5.03	1.98
18.20	16.56	7.66	3.02
19.24	17.51	6.92	2.72
19.89	18.10	7.37	2.90
20.57	18.72	7.12	2.80
20.84	18.96	8.81	3.47
21.17	19.27	9.48	3.73
21.77	19.81	1.00×10^{-3}	3.94
22.28	20.28	1.07	4.21
22.81	20.76	1.14	4.49
23.27	21.18	1.37	5.39
23.75	21.61	1.64	6.46
24.20	22.02	1.92	7.56
24.66	22.44	2.14	8.42
25.19	22.92	2.40	9.45
25.58	23.28	2.59	1.02×10^{-4}
26.12	23.77	2.77	1.09
26.64	24.24	3.06	1.20
27.26	24.81	3.40	1.34
27.74	25.24	4.00	1.57
28.15	25.62	4.64	1.83
28.61	26.04	5.29	2.08
29.21	26.58	6.03	2.37
30.26	27.54	2.19×10^{-2}	8.62

END

FILMED

3

-86

DTIC